© 2022. Published by The Company of Biologists Ltd | Development (2022) 149, dev199363. doi:10.1242/dev.199363

RESEARCH ARTICLE

Coordinated activities of Myosin Vb isoforms and mTOR signaling regulate epithelial cell morphology during development

Kirti Gupta, Sudipta Mukherjee*, Sumit Sen and Mahendra Sonawane‡

ABSTRACT

The maintenance of epithelial architecture necessitates tight regulation of cell size and shape. However, mechanisms underlying epithelial cell size regulation remain poorly understood. We show that the interaction of Myosin Vb with Rab11 prevents the accumulation of apically derived endosomes to maintain cell-size, whereas that with Rab10 regulates vesicular transport from the trans-Golgi. These interactions are required for the fine-tuning of the epithelial cell morphology during zebrafish development. Furthermore, the compensatory cell growth upon cell-proliferation inhibition involves a preferential expansion of the apical domain, leading to flatter epithelial cells, an efficient strategy to cover the surface with fewer cells. This apical domain growth requires post-trans-Golgi transport mediated by the Rab10-interacting Myosin Vb isoform, downstream of the mTOR-Fatty Acid Synthase (FASN) axis. Changes in trans-Golgi morphology indicate that the Golgi synchronizes mTOR-FASN-regulated biosynthetic input and Myosin Vb-Rab10 dependent output. Our study unravels the mechanism of polarized growth in epithelial cells and delineates functions of Myosin Vb isoforms in cell size regulation during development.

KEY WORDS: Cell size regulation, Compensatory cell growth, Tissue homeostasis, Myosin Vb, mTOR signaling, Epidermis, Zebrafish

INTRODUCTION

Epidermis is a stratified epithelium, which acts as a physical and biological barrier to protect the interior milieu in metazoans. To acquire and maintain the architecture of such a tissue, tight regulation of cellular attributes such as cell size, cell number and cell morphology is crucial (Gómez-Gálvez et al., 2018; Hannezo et al., 2014; Park et al., 2015). Epithelial cells display a high degree of homogeneity in terms of size and shape (Ginzberg et al., 2015; Puliafito et al., 2017; Sugimura and Ishihara, 2013), and irregularity in cell size may indicate a tissue anomaly (Ginzberg et al., 2015; Lloyd, 2013). In the epidermis, squamous cell morphology possibly allows efficient coverage of large surface area. Furthermore, under conditions like wounding, mechanical stretch and inhibition of cell proliferation, epidermal cells grow in size (Razzell et al., 2014; Sonal et al., 2014; Tamori and Deng, 2014). Whether such growth involves the acquisition of specific cell morphology and how such cell growth is regulated remains unclear.

Department of Biological Sciences, Tata Institute of Fundamental Research, Homi Bhabha Road, Mumbai 400005, India.
*Present address: Department of Physiology, Development and Neuroscience, University of Cambridge, Downing Street, Cambridge CB2 3EL, UK.

‡Author for correspondence (mahendras@tifr.res.in)

K.G., 0000-0002-0083-1926; M.S., 0000-0002-1749-6247

Handling Editor: Steve Wilson
Received 16 December 2020; Accepted 27 January 2022

Myosin Vb, an actin based motor, functions in the maintenance of epidermal cell size, by regulating plasma membrane homeostasis (Sonal et al., 2014). It consists of a head domain having ATPase activity and three well-characterized tail domains which bind to Rab8a, Rab10 and Rab11a to mediate exocytosis, membrane biogenesis and recycling, respectively (Lapierre et al., 2001; Liu et al., 2013; Roland et al., 2011). In intestinal epithelial cells, loss of Myosin Vb promotes bulk endocytosis from the apical surface (Engevik et al., 2019), contributing to the pathophysiology of Microvillus inclusion disease (MVID) (Müller et al., 2008; Ruemmele et al., 2010). The Myosin Vb-Rab8 interaction is required for proper microvilli formation, whereas disruption of its interaction with Rab11 results in apical membrane internalization and formation of microvillus inclusions (Knowles et al., 2014). Two functional isoforms have been identified for Myosin Vb; one containing Rab10-, Rab8- and Rab11-binding domains and the other having only Rab8- and Rab11-binding domains (Roland et al., 2009). In rat hippocampal and cortical neurons and zebrafish retinal ganglion cells, interaction of Myosin Vb with Rab10 promotes copious post-mitotic growth in axons (Liu et al., 2013). The role of Myosin Vb in membrane biogenesis in epithelial cells has not been explored so far.

Acquisition of cell size and its maintenance requires synthesis of plasma membrane components. In mammalian cells, *de novo* fatty acid synthesis contributes to membrane biogenesis during mitotic expansion and formation of cellular protrusions (Scaglia et al., 2015; Zhang et al., 2017). Key genes controlling membrane biogenesis, such as *fatty acid synthase* (*fasn*), are regulated by mTOR signaling (Yan et al., 2014; Yoon et al., 2007). mTORC1, along with other metabolic cues, governs the expression of FASN and other lipid biogenic enzymes via sterol regulatory element binding proteins (SREBPs) (Eberlé et al., 2004; Laplante et al., 2009; Madison, 2016; Peterson et al., 2011; Porstmann et al., 2008; Wen et al., 2012). Because of its central role in lipid as well as protein biosynthesis, mTOR signaling regulates cell size and tissue growth in various systems (Boehlke et al., 2010; Jones et al., 2009; Kuo et al., 2015; Tumaneng et al., 2012). So far, the role of mTOR-FASN-mediated membrane biogenesis in the acquisition or maintenance of cell size in the epidermal cells has remained unclear. Besides, it is poorly understood whether membrane biosynthesis coordinates with the cellular transport machinery in targeting the newly synthesized components to the plasma membrane during cell growth.

Using developing zebrafish epidermis as a model, we show that the interactions of Myosin Vb with Rab11 and Rab10 regulate different transport modes to maintain the epithelial cell morphology during development. Our analyses further reveal that the compensatory growth in the epidermal cells is characterized by a preferential increase in the apical domain – an efficient strategy to cover a large surface – and is regulated by mTOR and FASN. Interestingly, Myosin Vb-Rab10 interaction is essential for this

Development (2022) 149, dev199363. doi:10.1242/dev.199363

polarized growth of the epidermal cells. Our investigation further establishes a hierarchical connection between mTOR-FASN-mediated membrane biogenesis and directional vesicle transport via Myosin Vb during cell growth, with the trans-Golgi acting as an intermediate reservoir.

RESULTS

Importance of Myosin Vb-Rab11 and Myosin Vb-Rab10 interactions in the developing epidermis

The *gsp/myosin Vb* mutants and morphants expressing truncated versions of Myosin Vb – devoid of the complete tail domain – exhibit increased endocytosis and accumulation of early, recycling and late endosomes and lysosomes. This leads to increased membrane influx, perturbed membrane homeostasis and subsequent reduction in total cell surface area in zebrafish peridermal or outer epidermal cells. As a consequence, some of the peridermal cells round up and form clusters on the head and flank region (Phatak et al., 2021; Sonal et al., 2014).

To unravel the importance of Myosin Vb-Rab10 and MyosinVb-Rab11 interactions in the developing zebrafish epidermis, we aimed at rescuing the Myosin Vb deficiency by injecting mRNAs for: (1) full-length Myosin Vb having both Rab10- as well as Rab11-binding abilities; (2) an isoform of Myosin Vb without Rab10-binding domain; (3) Myosin Vb mutant lacking Rab11-binding ability; and (4) Myosin Vb incapable of binding to Rab10 and Rab11 (see Materials and Methods). Hereafter, these four conditions are referred to as MyoVb-Rab10^{+}/Rab11^{+}, MyoVb-Rab10^{-}/Rab11^{+}, MyoVb-Rab10^{+}/Rab11^{-} and MyoVb-Rab10^{-}/Rab11^{-}. To generate functional deficiency of Myosin Vb, we injected a previously validated splice site morpholino (Sonal et al., 2014) into a transgenic line *Tg(cldnB:lynEGFP)* in which peridermal cell membranes are marked with lyn-EGFP. Supplementing *myosin Vb* morphants by mRNAs for MyoVb-Rab10^{+}/Rab11^{+} and MyoVb-Rab10^{-}/Rab11^{+} rescued the morphological cell rounding phenotype (Fig. 1A,B) as well as previously reported (Sonal et al., 2014) cellular phenotypes, such as loss of microridges, reduction in cell size and accumulation of vesicles (Fig. 1C). In *myosin Vb* morphants, peridermal cells exhibit accumulation of apically derived endosomes arising from fluid-phase endocytosis as revealed by dextran uptake assay. This phenotype is rescued when embryos are supplemented with mRNA for MyoVb-Rab10^{+}/Rab11^{+} and MyoVb-Rab10^{-}/Rab11^{+} (Fig. S1B). Interestingly, injections of mRNAs for MyoVb-Rab10^{+}/Rab11^{-} and MyoVb-Rab10^{-}/Rab11^{-} rescued neither the morphological nor the cellular phenotypes (Fig. 1A,C; Fig. S1B), suggesting that whereas Myosin Vb and Rab11 interaction is essential for maintenance of cell size and shape, the interaction of Myosin Vb with Rab10 is apparently dispensable for this process. However, staining with wheat germ agglutinin (WGA), which marks the trans-Golgi network (TGN) and post-TGN vesicles (Kanazawa et al., 2008), revealed that the injection of mRNA for MyoVb-Rab10^{-}/Rab11^{+} in Myosin Vb-deficient embryos – but not for MyoVb-Rab10^{+}/Rab11^{+} – results in a Golgi phenotype characterized by the increased branching of the trans-Golgi and large WGA-positive vesicles closely apposed to the trans-Golgi (Fig. 1C). The radiating long-branched trans-Golgi was more obviously present. Embryos showing the Golgi phenotype in a larger proportion of epidermal cells (more than ∼40-50%) were counted as embryos showing Rab10-binding deficiency phenotype. Although the penetrance varied across experimental sets, the number of embryos showing the Golgi phenotype could reach up to 70% in the *myosin Vb* morphants rescued with Rab10^{-}/Rab11^{+} mRNA (Fig. 1D).

To confirm that the cellular phenotype is because of the predicted perturbation in either Rab10 or Rab11 binding, we selectively rescued the *myosin Vb* morphants with either MyoVb-Rab10^{+}/Rab11^{-} or MyoVb-Rab10^{-}/Rab11^{+} mRNA and analyzed the accumulation of Rab10 and Rab11 labeled vesicles (Fig. S2). We observed the partial rescue of Rab11 vesicles in MyoVb-Rab10^{-}/Rab11^{+}-injected morphants (Fig. S2C,D; Kruskal–Wallis test with Dunn's post hoc test, $P<0.05$), whereas the Golgi phenotype with Rab10 vesicle accumulation was present mostly in MyoVb-Rab10^{-}/Rab11^{+}-injected morphants (Fig. S2A,B). It is important to note that MyoVb-deficient embryos and the MyoVb-deficient embryos injected with MyoVb-Rab10^{+}/Rab11^{-} mRNA did not exhibit a higher number of Rab10 vesicles. In both these conditions, trans-Golgi showed highly perturbed organization (Fig. S2A) presumably due to massive accumulation of late endosomes and lysosomes (Sonal et al., 2014). This may either affect the biogenic function of the Golgi or result in a faster clearance of post-TGN vesicles.

To conclude, the phenotypic features seen in Myosin Vb-deficient embryos, such as increased endosome accumulation, reduction in cell surface area, cell rounding up and loss of apical microridges, are attributed to the loss of Myosin Vb-Rab11 interaction, whereas the Golgi phenotype may be attributed to the loss of Myosin Vb-Rab10 interaction.

Knockdown of Rab10-binding isoform of Myosin Vb results in a bigger and branched trans-Golgi and an accumulation of post-trans-Golgi vesicles

The Golgi phenotype in Myosin Vb-deficient embryos rescued with mRNA for MyoVb-Rab10^{-}/Rab11^{+} was intriguing and suggested the role of Myosin Vb-Rab10 interaction in the post-TGN traffic. We reasoned that investigating this phenotype would lead towards an understanding of the functional importance of the Myosin Vb-Rab10 interaction in the epithelial cells. As the penetrance of the Golgi phenotype in the rescued embryos varied, we used a previously published splice site morpholino for this purpose. This morpholino prevents the inclusion of Exon D – which encodes the Rab10-binding domain – into the transcript, selectively knocking down the Myosin Vb isoform consisting of the Rab10-binding domain (Liu et al., 2013). Our RT-PCR analysis confirmed that the morpholino indeed knocked down Exon D-containing *myosin Vb* transcripts (Fig. S3A) and is henceforth referred to as Exon D MO. The previously reported optic nerve thinning phenotype (Liu et al., 2013) in the Exon D morphant was also present in the *gsp*^{NS042} (*myosin Vb*) mutant embryos as well as in the *myosin Vb* morphants (Fig. S3B).

To delineate the function of the Rab10-binding isoform of Myosin Vb in the epidermis, we characterized the Exon D morphant phenotype. The morphological phenotype was characterized by a slight reduction in the head size and reduced tail fin expansion. No epidermal defects were observed at the morphological level (Fig. 2A). To characterize the trans-Golgi morphology in morphant embryos, we marked the trans-Golgi compartment with a plasmid-encoded EGFP-tagged trans-Golgi-resident enzyme galactose-1-phosphate uridylyltransferase (EGFP-GalT) (Gupta and Sonawane, 2020; Nilsson et al., 1993; Rabouille et al., 1995; Sepich and Solnica-Krezel, 2016) and WGA, which marks both TGN and vesicles derived from TGN (Kanazawa et al., 2008). In Exon D-deficient embryos, the trans-Golgi appeared to be larger and highly branched. In addition, large post trans-Golgi vesicles – labeled only by WGA, but not with GalT – were closely apposed to trans-Golgi, and this phenotype appeared to be the most severe at 36 h post-fertilization (hpf) (Fig. 2B). This analysis suggested that the differentiated post trans-Golgi vesicles (WGA labeled but GalT

Development (2022) 149, dev199363. doi:10.1242/dev.199363

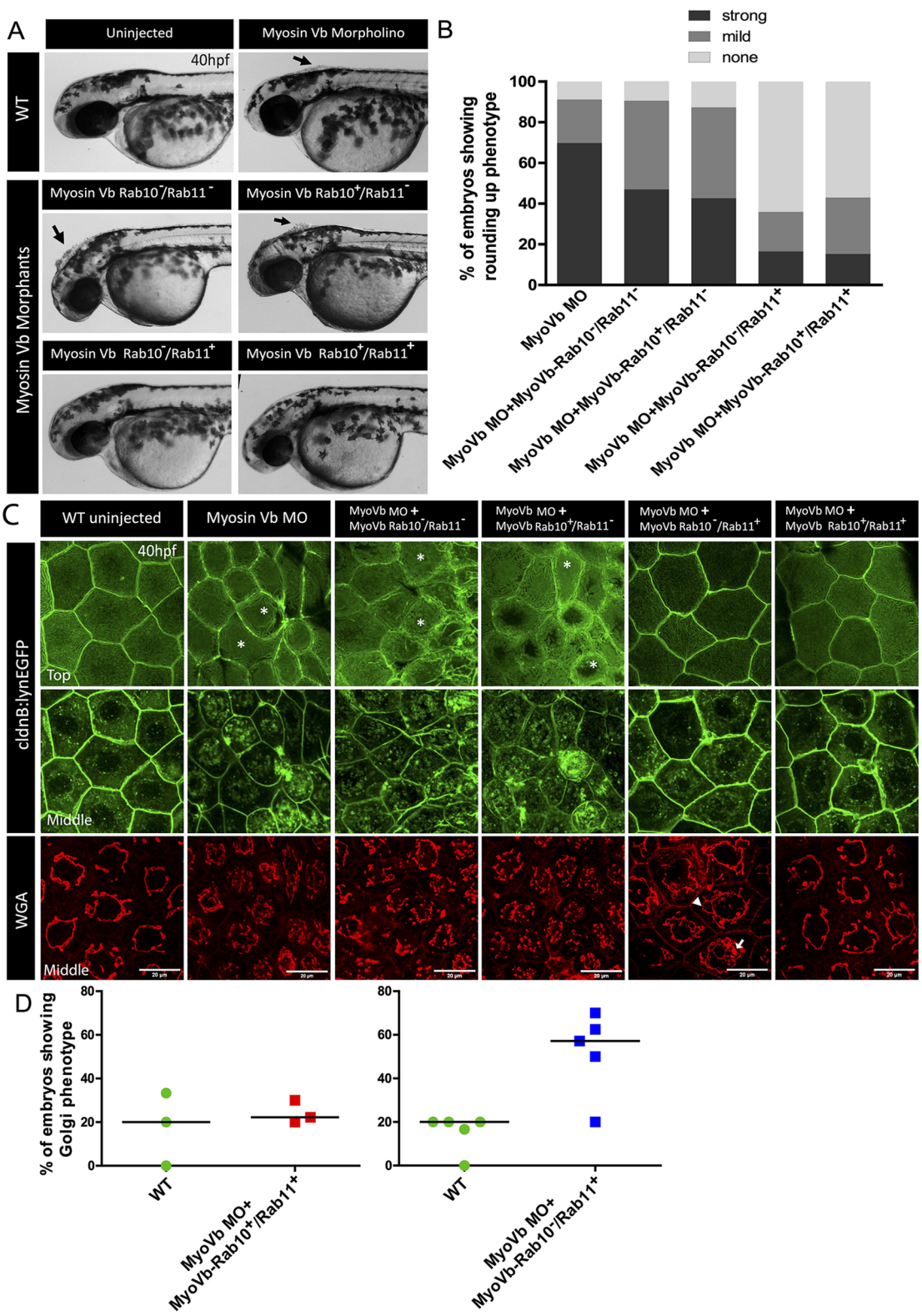

Fig. 1. Myosin Vb-Rab11 interaction is essential to maintain cell size and shape, whereas Myosin Vb-Rab10 interaction controls trans-Golgi morphology. (A) Representative brightfield images of Myosin Vb morphants at 40 hpf, with and without compensation with mRNA encoding different Myosin Vb isoforms mentioned in the figure. (B) Graphical representation of proportion of Myosin Vb morphants (MyoVb MO) showing either strong, mild or no cell rounding phenotype upon injections of mRNA for the mentioned Myosin Vb isoforms. (C) Confocal images of the 40 hpf morphant peridermal cells in *Tg(cldnB:lynEGFP)* transgenic line with the membrane and the vesicles marked with Lyn-GFP and trans-Golgi marked with WGA (top panel confocal *z*-stack at 0 µm; middle panel *z*-stack at 1.9-2.2 µm). (D) Percentage of the morphant embryos showing trans-Golgi phenotype characterized by branching of trans-Golgi and the presence of large vesicles in the morphant embryos injected with mRNA for stated Myosin Vb isoforms. Black arrows in A show bunches of rounded-up cells. White arrow and arrowhead in C indicate a trans-Golgi vesicle and branch, respectively. Asterisks in C point to the absence of microridges in the apical domain of the peridermal cells. Horizontal bar shows mean. Scale bars: 20 µm (C).

Development (2022) 149, dev199363. doi:10.1242/dev.199363

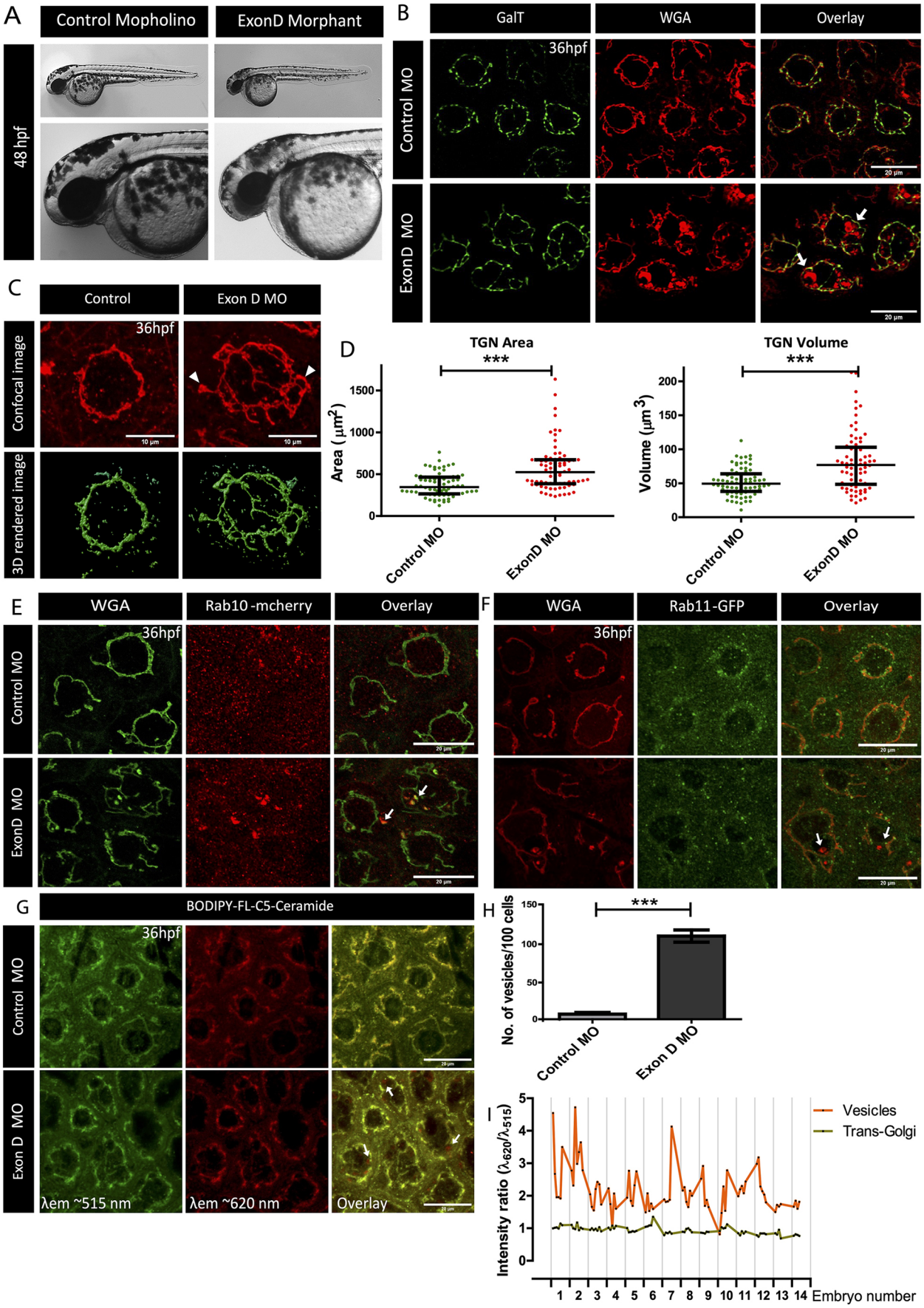

Fig. 2. See next page for legend.

Development (2022) 149, dev199363. doi:10.1242/dev.199363

Fig. 2. Myosin Vb Exon D knockdown results in increased trans-Golgi branching and accumulation of post-TGN vesicles in the peridermal cells. (A) Brightfield images of control and Exon D morphants (Exon D MO) at 48 hpf show that knockdown of Exon D isoform (Rab10 binding) does not result in rounded up cells in the head region. (B) Confocal images of peridermal cells of the control (Control MO) and Exon D morphants (Exon D MO) at 36 hpf immunostained for GalT-GFP and trans-Golgi using WGA. (C,D) 3D rendering of TGN by Huygen's software (C) followed by quantification (D) revealed an increase in both surface area and volume of the TGN. (E,F) Confocal stacks of control and Exon D morphants stained for trans-Golgi (WGA) and Rab10 (E) and trans-Golgi (WGA) and Rab11 (F). (G-I) Confocal micrographs of BODIPY-FL-C_5-Ceramide-labeled peridermal cells from control and Exon D morphants at 36 hpf, imaged using λex=488 nm and λem at ∼515 nm (green) and ∼620 nm (red) (G) followed by quantification of number of vesicles (H), and intensity ratio of red:green fluorescence of large Ceramide-rich compartments ['red' appearing vesicles in overlays (G)] as well as the TGN (I). White arrows in B, E-G point to trans-Golgi vesicles in overlay panels. White arrowheads in C point to trans-Golgi branches. Data are median±interquartile range. ***P<0.001 (Mann–Whitney U test; Table S1). Scale bars: 20 µm (B,E-G); 10 µm (C).

negative) accumulate at the trans-Golgi, possibly owing to the absence of further transport. Quantifications using 3D deconvoluted images of WGA-stained TGN (Fig. 2C; see Materials and Methods for details) revealed a statistically significant increase in the surface area and volume of TGN in the peridermal cells of Exon D morphants (Fig. 2D; Mann–Whitney U-test, P<0.05). To verify the specificity of the morpholino, we rescued the Golgi phenotype in Exon D morphants by injecting mRNA for MyoVb-Rab10^{+}/Rab11^{+} in a clonal manner. We observed qualitative as well as quantitative rescue of the TGN phenotype specifically in the mRNA clones compared with the neighboring non-clonal cells that were deficient for the Exon-D isoform and did not receive mRNA for MyoVb-Rab10^{+}/Rab11^{+}. Notably, we did not observe the rescue in TGN phenotype when mRNA for MyoVb-Rab10^{-}/Rab11^{+} was used for the clonal analysis (Fig. S3C,D; Kruskal–Wallis test with Dunn's post hoc test, P<0.05). We also confirmed the TGN phenotype using the second splice morpholino to knock down the Exon D isoform (Fig. S3E).

To test whether transport of Rab10 vesicles is specifically disrupted, we injected Rab10-mCherry mRNA into the control and Exon D morphants, and visualized the Rab10 vesicles both in live and in fixed samples co-stained with WGA. Live imaging of the periderm revealed that larger Rab10 vesicles were exclusively present in Exon D morphants (Fig. S3F). In fixed preparations, most of these large Rab10-mcherry labeled vesicles showed co-staining with WGA and were located in the peri-Golgi region (Fig. 2E). Further analysis using the *Tg(h2afx:EGFP-Rab11a)*^{mw6} transgenic line (Clark et al., 2011) revealed that Rab11-labeled endosomes did not co-localize with WGA in Exon D morphants (Fig. 2F). These analyses suggest that most of the large post-TGN vesicles are Rab10 compartments that accumulate owing to absence of the Rab10-interacting Myosin Vb isoform. To ascertain the nature of these post-TGN vesicles, we pulse labeled embryos with BODIPY-FL-C_5-Ceramide followed by imaging of the periderm. Enrichment of this BODIPY-FL-C5-Ceramide dye in sphingolipid-rich biogenic compartments results in a shift in its λ_{em} from ∼515 nm (green) to ∼620 nm (Pagano et al., 1991). In the Exon D morphant embryos, we observed large vesicles juxtaposed to the trans-Golgi showing increased emission at 620 nm (Fig. 2G,H; Mann–Whitney U-test, P<0.05), suggesting their enrichment with sphingolipids. This BODIPY-FL-C5-Ceramide enrichment in the vesicles was clearly discernible when an intensity ratio of λ_{620} nm/λ_{515} nm was compared between the vesicles and TGN (Fig. 2I).

We further investigated the fate of the large vesicles that accumulate at the trans-Golgi surface. We reasoned that these vesicles would acquire late endo-lysosomal fate for the cells to reuse the accumulated vesicular contents. To test this idea, we knocked down the Exon D isoform in a transgenic line *Tg(h2afx:EGFP-Rab7)*^{mw7} that expresses EGFP-tagged Rab7 (Clark et al., 2011). Strikingly, large Rab7-labeled compartments were observed in Exon D morphants, compared with smaller Rab7-labeled vesicles seen in controls (Fig. S4A). Further immunostaining analysis revealed that the accumulated post-TGN vesicles labeled by WGA were co-stained for Rab7 and LAMP-1 – a lysosomal marker – in the Exon D morphants at 36 hpf (Fig. S4B). This indicates endo-lysosomal processing of the vesicular load accumulated around Golgi in the absence of the Exon D isoform. Consistent with this observation, the temporal analysis revealed that the size and number of the vesicles increase from 22 hpf to 36 hpf and decrease thereafter by 72 hpf (Fig. S4C,D; Kruskal–Wallis test with Dunn's post hoc test, P<0.05).

To conclude, in the absence of the Myosin Vb-Rab10 interaction, afferent transport from the trans-Golgi is inhibited, resulting in increased TGN size as well as accumulation of Rab10-labeled and sphingolipid-rich, presumably biogenic, vesicles that remain apposed to the trans-Golgi surface. In the absence of their further transport, the accumulated vesicles acquire late endosomal-lysosomal fate, gradually degrading the contents.

Compensatory growth of peridermal cells involves preferential expansion of the apical domain and requires the Rab10-binding isoform of Myosin Vb

Membrane biogenesis involves *de novo* synthesis of membrane lipids and their transport from trans-Golgi to plasma membrane. As we observed accumulation of sphingolipid-rich vesicles in the vicinity of trans-Golgi, we asked whether epidermal cells display reduction in cell size in the absence of this Exon D-containing isoform. To test this, we injected the Exon D morpholino in the embryos from *Tg(cldnB:lynEGFP)* transgenic line and quantified the total surface area of the peridermal cells. To our surprise, the Exon D morphants showed a slight increase in the basolateral surface area as well as cell height, whereas the apical surface remained unchanged, yielding a taller morphology (Fig. 3A,B; Mann–Whitney U-test, P<0.05). The marginal increase observed in the total surface can plausibly be attributed to the increase in the basolateral surface area. These data suggest that the Rab10-binding isoform of Myosin Vb is essential to maintain the cell morphology but does not have a major developmental function in cell size determination in the epidermis.

We further asked whether the function of the Rab10-binding Myosin Vb isoform becomes essential when the epidermal cells undergo hypertrophy. To test this, we used previously established paradigms (Sonal et al., 2014) to achieve compensatory cell growth by inhibiting cell proliferation by downregulation of EGFR signaling using PD 168393 and knockdown of ΔNp63 transcription factor (Bakkers et al., 2002; Lee and Kimelman, 2002; Sonal et al., 2014). Interestingly, the reduction in cell proliferation results in an anisometric growth, wherein ∼30-50% increase in the apical surface contributes towards cell expansion (Fig. 3C,D; Kruskal–Wallis test with Dunn's post hoc test, P<0.05). The basolateral membrane increased by ∼10% in this experiment (Fig. 3C,D), but the increase appears to vary between 4-25% in the other experiments reported in this study and was not always statistically significant (e.g. Fig. 3F). As the apical growth is much larger than the basolateral growth, the height of the cells does not increase. This results in flatter peridermal

Development (2022) 149, dev199363. doi:10.1242/dev.199363

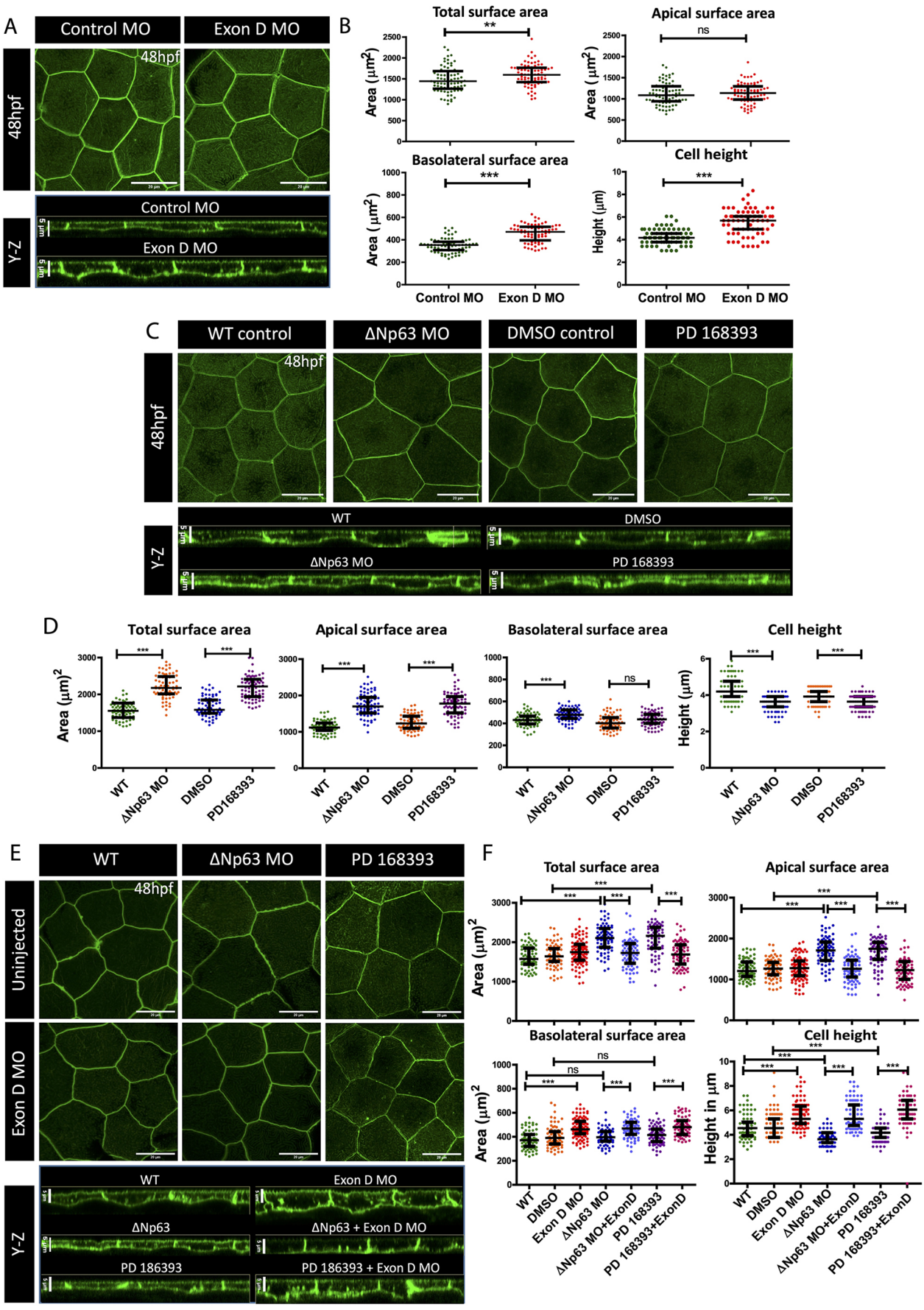

Fig. 3. See next page for legend.

Development (2022) 149, dev199363. doi:10.1242/dev.199363

Fig. 3. Rab10-interacting isoform of Myosin Vb regulates cell morphology during development and is essential for the apical domain expansion during compensatory cell growth. (A,C,E) Confocal scans and orthogonal (Y-Z) sections of the peridermal cells at 48 hpf of immunostained embryos of *Tg(cldnB:lynEGFP)* line injected with control (Control MO) and Exon D morphants (Exon D MO) (A), upon knockdown of ΔNp63 (ΔNp63 MO) and inhibition of EGF signaling by treatment with PD168393 (C) or uninjected or Exon-D morphants injected with ΔNp63 morpholino or treated with PD168393 (E). (B,D,F) Graphical representation of quantification of total, apical and basolateral surface area, and the cell height, under given genetic conditions or treatments in A,C,E, respectively. Data are median±interquartile range. $^{**}P<0.01$, $^{***}P<0.001$ [Mann–Whitney U test (B); Kruskal–Wallis test with Dunn's post hoc test (D,F)]. ns, not significant. Note that only essential paired comparisons are shown in D and F using horizontal line segments. For the details of all the comparisons please refer to Table S2. Scale bars: 20 µm (X-Z plane of A,C,E, top panels); 5 µm (Y-Z plane of A,C,E, bottom panels).

cells having a large cross-sectional area (Fig. 3C). Notably, the Exon D morphants were unable to display compensatory hypertrophy and showed inability to grow the apical domain, but the basolateral membrane and cell height were able to grow (Fig. 3E,F; Kruskal–Wallis test with Dunn's post hoc test, $P<0.05$).

To conclude, compensatory cell growth involves selective increase in the apical surface, which results in peridermal cells acquiring flatter morphologies. The Exon D isoform of Myosin Vb, although dispensable for cell size regulation in the developing epidermis, becomes essential for the apical membrane growth during compensatory hypertrophy.

Cellular hypertrophy in the periderm is regulated cooperatively by mTOR signaling and Rab10-dependent Myosin Vb transport

The cell surface area increase under the proliferation inhibition condition presents a compensatory hypertrophy paradigm with 30-40% increase in the total surface area. We asked how membrane biogenesis is regulated during this cell-growth and whether the Rab10-binding isoform of Myosin Vb cooperates with the membrane biogenic pathway. We checked the status of lipid anabolism by looking at levels of one of the essential and key enzymes of the *de novo* lipid synthesis pathway, FASN, which is required for the growth of the plasma membrane (Knobloch et al., 2013; Paoletti et al., 2007; Schuller et al., 1992; Vadia et al., 2017; Yao et al., 2012; Zhang et al., 2017). Under both the paradigms of compensatory cell size increase, FASN levels showed an upregulation (Fig. 4A,B; Mann–Whitney *U*-test, $P<0.05$). To confirm the role of FASN in cell size increase, we inhibited the function of FASN using Cerulenin (Kawaguchi et al., 1982; Omura, 1976; Vance et al., 1972). We observed a qualitative decrease in FASN levels in the peridermal cells (Fig. S5A). In addition, Cerulenin treatment led to an overall reduction in the peridermal cell size, with a prominent decrease in the apical domain in control embryos as well as in the embryos treated with EGFR inhibitor or injected with ΔNp63 morpholino, whereas the decrease in the size of the basolateral domain was marginal (Fig. 4C,E; Kruskal–Wallis test with Dunn's post hoc test, $P<0.05$).

mTOR signaling is a master regulator of metabolism, and controls lipid synthesis by regulating SREBP-dependent fatty acid synthesis (Peterson et al., 2011; Porstmann et al., 2008; Soliman, 2011; Yoon et al., 2007). We found that treatment with Rapamycin – an established mTOR inhibitor – resulted in downregulation of phospho-ribosomal protein S6 (pS6; a known target of mTORC1) along with FASN in the zebrafish periderm (Fig. S5B,C). Although the Rapamycin treatment did not have an effect on the peridermal cell size in developing embryos, in proliferation-inhibition paradigms the Rapamycin-treated peridermal cells did not attain compensatory cell-hypertrophy and remained similar to those in the control embryos (Fig. 4D,F; Kruskal–Wallis test with Dunn's post hoc test, $P<0.05$).

The fact that both mTOR signaling and the Exon D isoform are required for compensatory growth indicates that these two components may have a cooperative relationship during cellular hypertrophy. To probe this notion, we established mTOR signaling activation paradigms using compound C – an AMPK inhibitor. Compound C reverses the effect of AMPK-induced reduction in FASN levels and increases the phosphorylation of acetyl-CoA carboxylase (ACC), thereby favoring lipogenesis (Fediuc et al., 2006; Fernández-Galilea et al., 2014; Zhou et al., 2001).

Compound C treatment resulted in an increase in the levels of pS6 as well as FASN (Fig. S6A,B). Quantification revealed a significant increase in total cell surface area in Compound C-treated embryos. In contrast to the proliferation-inhibition paradigms (Fig. 3F), here the membrane growth was proportional in both apical (25-35%) as well as basolateral surface area (30-40%) (Fig. S6C,D). Importantly, the Exon D morphants treated with compound C were unable to expand their apical surface. The basolateral area in these embryos showed a mild increase, which was statistically not significant, possibly because the increase due to the loss of the Exon D isoform is marginal over the increase resulting from compound C treatment. Nevertheless, we observed a significant increase in cell height in the Exon D morphants treated with compound C compared with the treated control embryos, likely a combined consequence of marginal increase in the basolateral area and reduced apical area (Fig. 5A,B; Kruskal–Wallis test with Dunn's post hoc test, $P<0.05$).

To conclude, our analyses indicate that compensatory hypertrophy requires mTOR-FASN-dependent membrane biogenesis. The Rab10-interacting isoform of Myosin Vb functions in mTOR-dependent polarized growth of peridermal cells. Our data indicate that vesicular transport by Myosin Vb-Rab10 at the trans-Golgi acts as a permissive step downstream of mTOR signaling during the regulation of epidermal cell growth.

Coordination between mTOR-FASN-mediated biosynthesis and Myosin Vb-mediated transport takes place at the TGN

Our analyses showed that the epidermal cell growth is regulated by coordinated activities of the membrane biosynthetic pathway and Myosin Vb. Given that newly synthesized membrane lipids such as phospholipids and sphingolipids are transported to the plasma membrane via trans-Golgi (Blom et al., 2011; Griffiths and Simons, 1986; Ikonen and Simons, 1998), and the fact that Myosin Vb function is required at the trans-Golgi surface, we hypothesized that the coordination would take place at the level of Golgi. If true, TGN morphology would alter depending upon the extent of input (synthesis) and output (transport from the TGN).

To test whether decreased biosynthesis would alter trans-Golgi morphology, we analyzed embryos treated with Rapamycin. This treatment resulted in a stark reduction in the TGN surface area, volume and trans-Golgi branching in the peridermal cells compared with control (Fig. 6A,C; Mann–Whitney *U*-test, $P<0.05$). Although the cell size did not decrease upon Rapamycin treatment (Fig. 6A,B; Mann–Whitney *U*-test, $P<0.05$), a stronger inhibition of mTOR signaling by Torin 1 (Liu et al., 2010; Thoreen et al., 2009) did result in a decrease in trans-Golgi branching, TGN size and cell size (Fig. S7A-C).

We further analyzed TGN morphologies linked with the cell size phenotypes under proliferation-inhibition paradigms, mTOR activation and proliferation-inhibition paradigms in combination with Exon D knockdown. In all the three conditions – EGFR

Development (2022) 149, dev199363. doi:10.1242/dev.199363

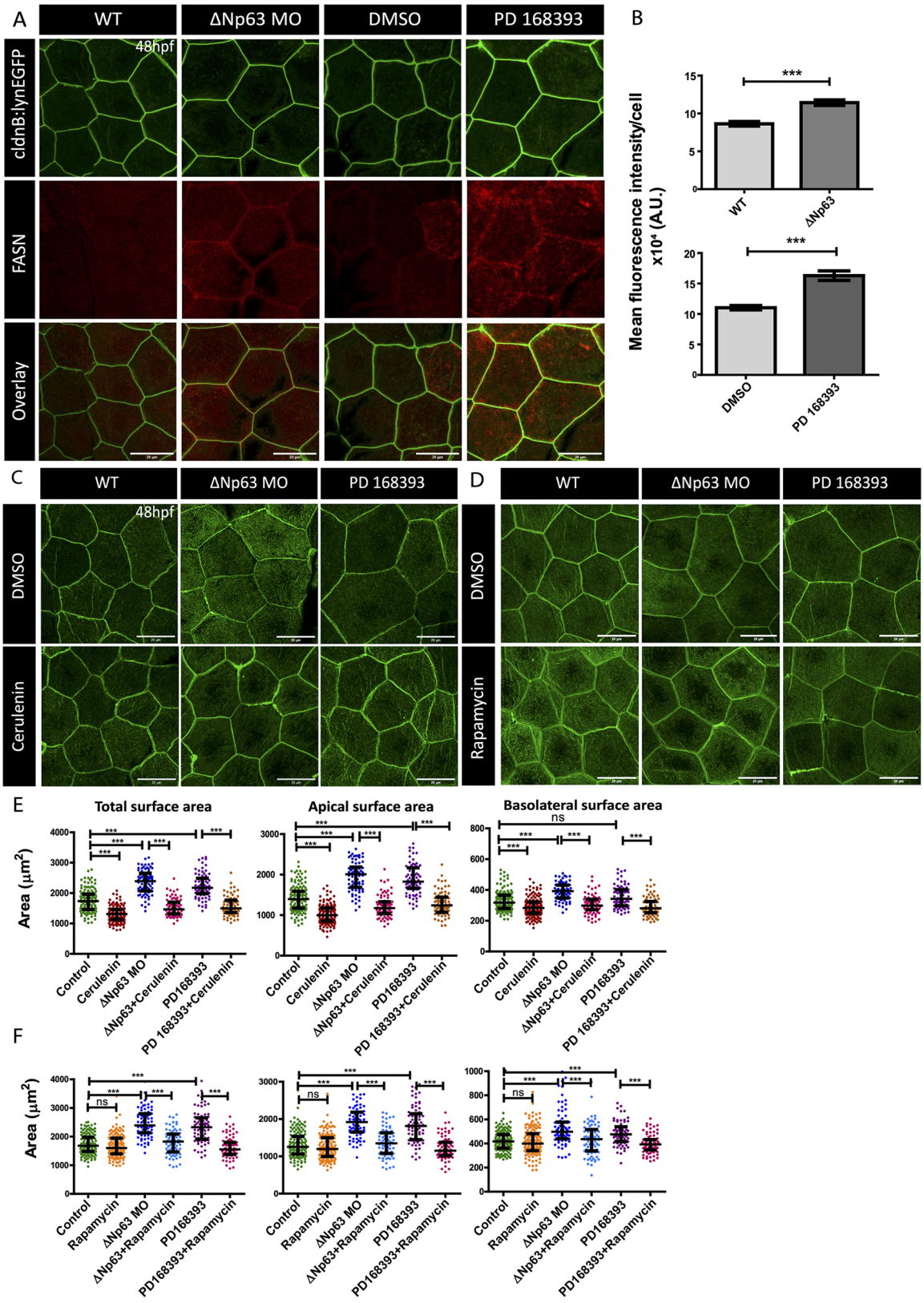

Fig. 4. Activity of FASN and mTOR is essential for compensatory cell growth in the developing periderm. (A,B) Immunostainings using anti-FASN antibody followed by confocal imaging (A) and fluorescence intensity quantification (B) in the embryos obtained from the *Tg(cldnB:lynEGFP)* line that are morphants for ΔNp63 (ΔNp63 MO) or treated with PD168393, and fixed at 48 hpf. (C-F) Confocal scans (C,D) and graphical representation of the total, apical and basolateral area quantifications (E,F) in ΔNp63 morphants (ΔNp63 MO) and PD168393-treated embryos upon FASN inhibition by Cerulenin (C,E) or mTOR inhibition by Rapamycin (D,F). Data are mean±s.e.m. (B) and median±interquartile range (E,F). ****P*<0.001 [Mann–Whitney U test (B); Kruskal–Wallis test with Dunn's post hoc test (E,F)]. ns, not significant. Please note that only important paired comparisons are shown. For the entire pair-wise analyses please refer to Table S3. Scale bars: 20 µm.

Development (2022) 149, dev199363. doi:10.1242/dev.199363

inhibition, ΔNp63 knockdown and mTOR activation – the trans-Golgi morphology showed increased branching, surface area and volume (Fig. 6D,E; Fig. S7D,E; Kruskal–Wallis test with Dunn's post hoc test, $P<0.05$), suggesting a tight correlation between increased lipid synthesis, trans-Golgi size and increased cell size. Embryos subjected to proliferation-inhibition paradigms when treated with Rapamycin or Cerulenin did not show an increase in TGN surface area and volume in the peridermal cells (Fig. 6F,G; Fig. S7F,G; Kruskal–Wallis test with Dunn's post hoc test, $P<0.05$), and showed inability to undergo compensatory growth (Fig. 4C-F). This analysis suggested that the size and branching of the trans-Golgi compartment in developing wild-type embryos, as well as those subjected to proliferation-inhibition paradigms, depends upon mTOR-FASN-dependent inputs, which are also essential for cell size maintenance and cell growth.

Results presented above indicate that the trans-Golgi shows an increase in size and branching due to increased lipid synthesis, which is essential to acquire and maintain cellular hypertrophy. However, in the Exon D morphants, though the accumulation of TGN vesicles was understandable, the increase observed in trans-Golgi size and branching (Fig. 2C,D) was puzzling. We asked whether this increase in TGN size is also a consequence of the increased membrane biosynthesis in Exon D morphants. Indeed, we found significant increase in FASN levels in Exon D morphant peridermal cells, suggesting a feedback upregulation of lipid biosynthesis under reduced anterograde trafficking from the Golgi (Fig. S8A,B; Mann–Whitney *U*-test, $P<0.05$). To understand the significance of such an upregulation in the lipid synthesis and TGN expansion, we treated Exon D morphants with Rapamycin. Upon treatment, Exon D morphants exhibited diminished branching and reduction in TGN size, while the large post trans-Golgi vesicles were still present (Fig. 7A,B; Kruskal–Wallis test with Dunn's post hoc test, $P<0.05$). Importantly, we found a significant reduction in the basolateral surface area and in cell height in Rapamycin-treated Exon D morphants, suggesting that the basolateral membrane growth in Exon D morphants is a consequence of the compensatory synthesis of membrane components and their delivery independent of Myosin Vb-mediated transport. Intriguingly, we also observed a slight reduction in the apical area in Rapamycin-treated Exon D morphant peridermal cells compared with the control embryos and Exon D morphants but not with the Rapamycin-treated embryos. It is possible that in wild-type embryos the apical domain is regulated cooperatively by both mTOR and the Exon D isoform, and that in Exon D morphants mTOR signaling-mediated but Myosin Vb-independent membrane biogenesis is essential for the maintenance of the apical domain (Fig. 7C,D; Kruskal–Wallis test with Dunn's post hoc test, $P<0.05$).

We further investigated the Golgi phenotypes in proliferation-inhibition and mTOR-activation paradigms combined with Exon D knockdown, wherein peridermal cells do not show cellular hypertrophy. We observed an increase in FASN level upon knockdown of the Exon D isoform under proliferation-inhibition conditions (Fig. S8C). Upon EGFR inhibition in Exon D morphants, the TGN surface area and volume also remained higher than uninjected controls (Fig. 7E,F; Kruskal–Wallis test with Dunn's post hoc test, $P<0.05$). We also observed the same trend upon mTOR activation in Exon D morphants (Fig. S8D,E). Intriguingly, this trend was not conserved for ΔNp63-Exon D

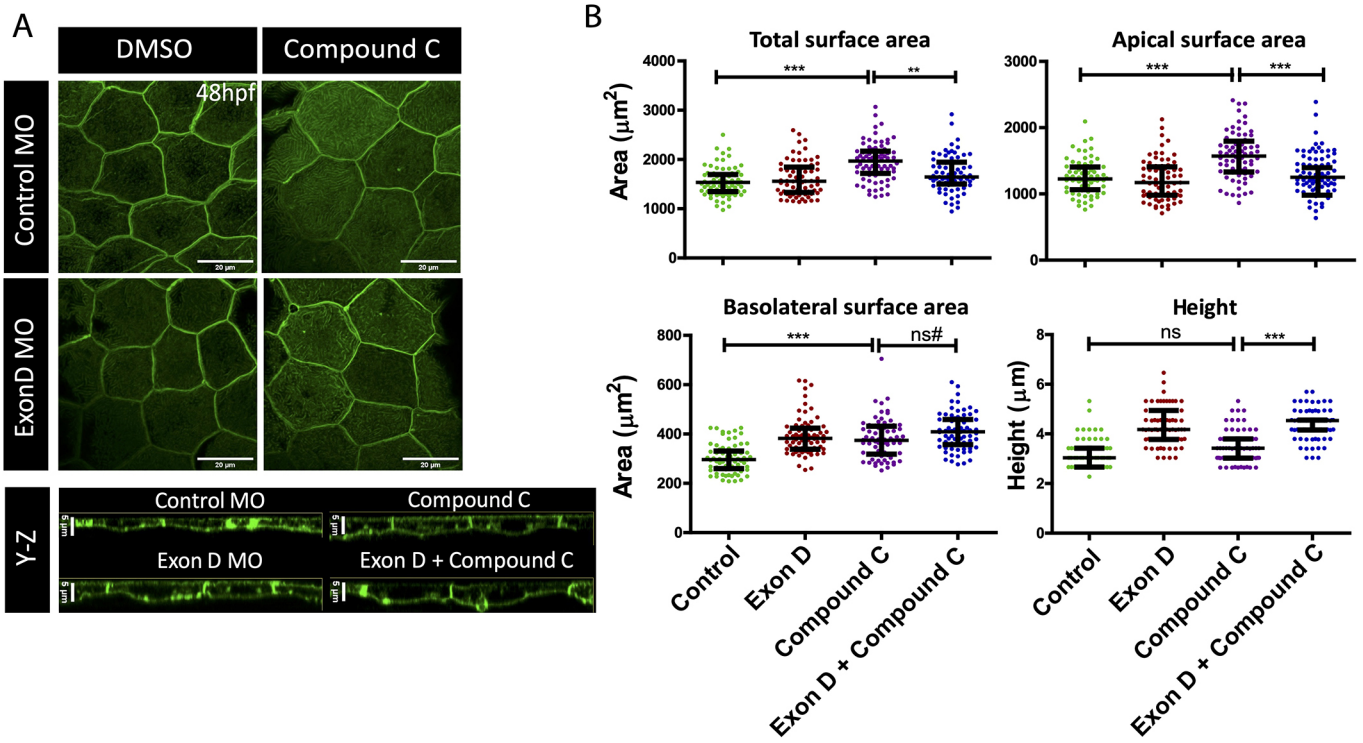

Fig. 5. Rab10-binding MyoVb isoform functions downstream of mTOR signaling during peridermal cell growth. (A) Confocal scans of lynEGFP-labeled peridermal cells of wild-type and Exon D morphant (Exon D MO) embryos treated with Compound C and DMSO at 48 hpf. (B) Graphical representation of the quantification of the total, apical and basolateral surface area, and the cell height in given genetic conditions and treatment. Data are median±interquartile range. **$P<0.01$, ***$P<0.001$ (Kruskal–Wallis test with Dunn's post hoc test). ns, not significant. ns#, although the difference is statistically not significant ($P=0.097$) the increasing trend might be biologically relevant (see the main text for details). Only key pairwise comparisons are shown in B; for the rest of the comparisons please refer to Table S4. Scale bars: 20 µm.

Development (2022) 149, dev199363. doi:10.1242/dev.199363

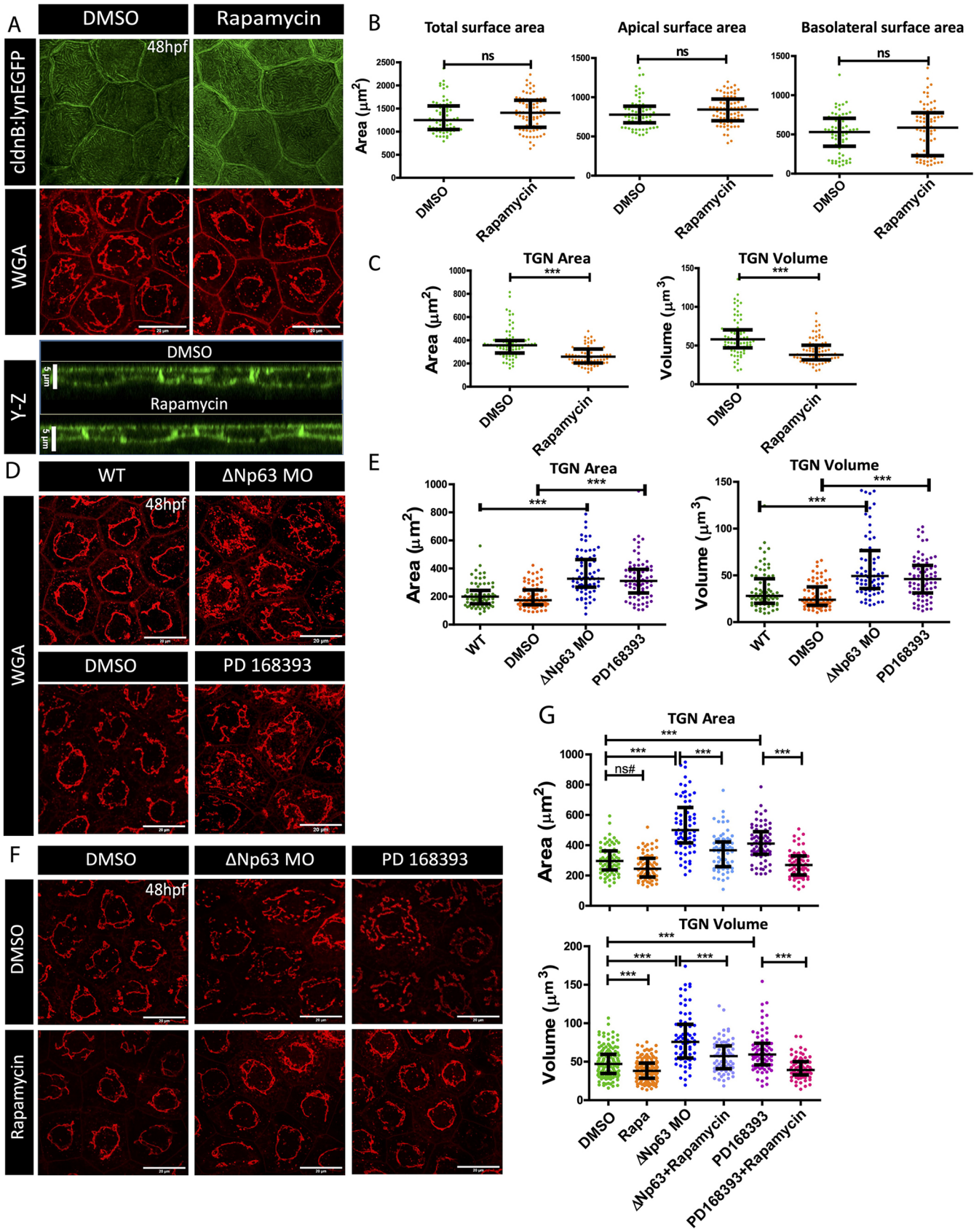

Fig. 6. See next page for legend.

Development (2022) 149, dev199363. doi:10.1242/dev.199363

Fig. 6. mTOR-mediated increase in the cell size corresponds to enlarged TGN size. (A) Confocal scans (X-Y and Y-Z planes) of the peridermal cells from 48 hpf embryos treated with DMSO (vehicle control) and Rapamycin and stained for lyn-EGFP and trans-Golgi (WGA). (B,C) Quantifications of total, apical and basolateral surface area (B), and TGN area and volume (C) upon Rapamycin treatment. (D,F) Confocal micrographs of TGN, labeled using WGA, from the peridermal cells from ΔNp63 morphants (ΔNp63 MO) and PD16393-treated embryos (D), and DMSO- or Rapamycin-treated ΔNp63 morphants and PD16393-treated embryos (F). (E,G) Graphical representation of TGN area and volume quantification in ΔNp63 morphants and PD16393-treated embryos (E), and DMSO or Rapamycin treated ΔNp63 morphants and PD16393-treated embryos (G). Data are median±interquartile range. ***P<0.001 [Mann–Whitney U test (B,C); Kruskal–Wallis test with Dunn's post hoc test (E,G)]. ns, not significant. ns$^{\#}$, although the comparison is not significant, the trend is similar to the other comparisons that have been seen to be statistically significant in other experiments (for example, in Figs 6C and 7B) performed in this study. Note that only essential pairwise comparisons are shown in panels E and G. A complete list of pairwise comparisons for B,C,E and G is given in Table S5. Scale bars: 20 µm (X-Y plane of A,D,F); 5 µm (Y-Z plane of A).

double morphants, in which we observed TGN surface area as well as volume to be comparable with that of the wild type (Fig. 7E,F). The absence of an increase in TGN surface area and volume in ΔNp63-Exon D double morphants is likely because of lysosomal processing of the accumulated cargo upon loss of ΔNp63 function and needs to be further investigated.

To conclude, the trans-Golgi compartment shows enlargement during compensatory cell growth and in the Exon D morphants. This enlargement is a consequence of the increased biosynthetic activity of mTOR-FASN axis. During the growth of the apical domain, the Exon D isoform acts downstream of the mTOR-FASN axis at the TGN. The increase in FASN levels in the absence of a functional Exon D isoform is a feedback response to increase membrane biogenesis. However, in the absence of Myosin Vb-Exon D, this compensatory growth is basolaterally directed.

DISCUSSION

Maintenance of the epithelial integrity is crucial for survival in metazoans. Under homeostatic conditions, epithelial cells maintain their morphology and number to conserve the tissue architecture. Whether and how epithelial cell morphologies are modulated under perturbed homeostatic conditions has remained unclear. In this study, we have unraveled the importance of interactions of Myosin Vb with Rab11 and Rab10 and its cooperativity with mTOR signaling in regulation of cell size in the developing zebrafish epidermis under normal and perturbed homeostatic conditions.

Our study shows that the interaction of Myosin Vb with Rab11 is of vital importance for the maintenance of epidermal cell size and shape during development. A complete rescue of the epidermal phenotype characterized by the restoration of cell size, cell shape and microridges was seen in Myosin Vb-deficient embryos supplemented with Myosin Vb that has the ability to interact with Rab11 but not with Rab10. Very interestingly, this also rescued the increased endosomal accumulation. It appears that MyosinVb-Rab11 interaction is essential to prevent either the excessive apical endocytosis or for clearing off the increased endocytic load by recycling it back to the plasma membrane (Fig. 7G). Recently, it has been shown that the apical endocytic flux in the absence of Myosin Vb is a cause of microvillus inclusions in enterocytes leading to MVID (Engevik et al., 2019; Sidhaye et al., 2016; Weis et al., 2016). Our data reveal that the disruption of Myosin Vb-Rab11 interaction results in apical inclusion in other epithelial systems such as the epidermis, and is not just restricted to the gut epithelium.

In many tissues such as liver, kidney, heart and cornea, the post-mitotic growth of the cells is observed upon reduction in the cell number. Such post-mitotic growth is known as compensatory cellular hypertrophy and is reported to be important for the restoration of the organ size and functionality (Tamori and Deng, 2014). In the absence of timely growth, the epithelial cells become stretched and flattened until the tissue breaks (Tamori and Deng, 2014). So far, cellular hypertrophy has been shown to be achieved via polyploidization, cell fusion and activation of metabolic signaling pathways (Al-Awqati, 2015; Haga et al., 2005; Honda et al., 1982; Losick et al., 2013; Tamori and Deng, 2013). Our results indicate that in an epithelial system, cells show preferential increase in the apical domain during hypertrophic growth (Fig. 7G). As a consequence of this directional growth, cells acquire flatter morphology and each cell covers a larger area. This is an effective strategy to cover a large surface with relatively fewer cells and by minimizing the energy expenditure on membrane synthesis.

How is the preferential apical growth regulated during cellular hypertrophy? Our data indicate that Myosin Vb and the mTOR pathway cooperate to achieve the preferential apical growth. Our analyses reveal that, in the absence of cell proliferation, cellular hypertrophy is driven by mTOR-dependent activity of FASN. The activation of mTOR by AMPK inhibition (compound C treatment) results in FASN-dependent cellular hypertrophy that is non-directional. The prominent effect of loss of the Exon D isoform on the apical domain in all these hypertrophy conditions indicates that Myosin Vb directs the transport of apical membrane components after their mTOR-dependent synthesis. Although the importance of Myosin Vb-Rab11 is well established in apically directed transport (Hobdy-Henderson et al., 2003; Khandelwal et al., 2013; Lapierre et al., 2001; Roland et al., 2011; Swiatecka-Urban et al., 2007; Vogel et al., 2015; Weisz and Rodriguez-Boulan, 2009), our report establishes for the first time that the interaction of Myosin Vb-Rab10 at the Golgi contributes to the growth of the apical domain (Fig. 7G). Our analyses reveal that biogenic vesicles generated at the Golgi depend on Myosin Vb-Rab10 interactions to get transported away from the Golgi to the plasma membrane to achieve compensatory cell growth. In the absence of these interactions, the biogenic vesicles accumulate at the Golgi, acquire endo-lysosomal fate and get cleared up from the cytoplasm. Such accumulation of Golgi-derived endo-lysosomal compartment, in the absence of appropriated transport of lipids from the Golgi, has been previously described (D'Souza et al., 2019; Robenek and Schmitz, 1991). Myosin Vb is an actin-based motor. We did observe short actin tracks near Golgi and actin punctae proximal to the trans-Golgi (K.G. and M.S., unpublished). It is likely that the transient actin polymerization around trans-Golgi vesicles allows the motor to pull these vesicles away from the Golgi and load them onto the microtubular cytoskeleton for further transport to the plasma membrane.

In the absence of the Rab10 interacting isoform of Myosin Vb, we observed accumulation of vesicles near the Golgi; however, there was no reduction in the size of the apical domain in the developing peridermal cells. Given that plasma membrane components are recycled and replenished as part of membrane surveillance mechanisms (Stefan et al., 2017), it is likely that, in the absence of Rab10-Myosin Vb interaction, such mechanisms are perturbed, leading to altered plasma membrane composition. In proliferation-inhibition conditions, cell expansion is essential to maintain the integrity. Our data indicate that the mTOR-FASN axis gets activated by either sensing the increased demand of plasma membrane components during cell growth or due to the altered plasma membrane attributes as a consequence of the disruption of transport

Development (2022) 149, dev199363. doi:10.1242/dev.199363

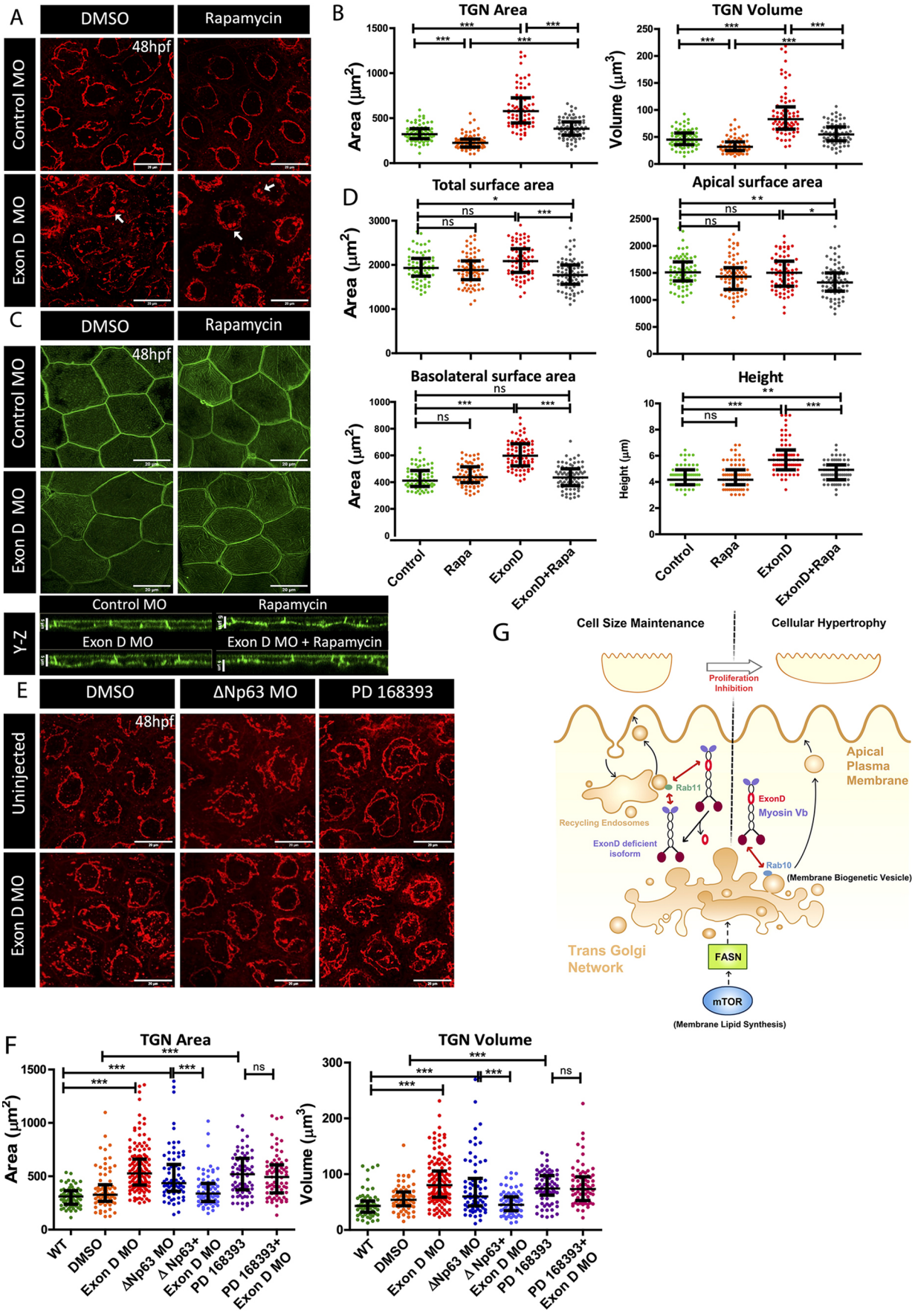

Fig. 7. See next page for legend.

Development (2022) 149, dev199363. doi:10.1242/dev.199363

Fig. 7. Myosin Vb and mTOR co-ordination at the TGN. (A,C) Confocal scans of the peridermal cells showing TGN (A) and cell membranes (C) of 48 hpf *Tg(cldnB:lynEGFP)* embryos injected with Exon D morpholino (Exon D MO) and the control embryos treated with DMSO or Rapamycin. (B,D) Quantification of the TGN surface area and volume (B) and total, apical and basolateral cell surface area and cell height (D) under different genetic conditions mentioned along the *x*-axes. (E,F) TGN morphologies (E) and quantifications of TGN surface area and volume (F) from the uninjected and Exon D morphant embryos either co-injected with ΔNp63 morpholino (ΔNp63 MO) or treated with PD16393 drug. (G) A schematic of Myosin Vb isoforms showing different outcomes depending upon their interaction with either Rab11 or Rab10. Although Myosin Vb-Rab11 interaction is essential to maintain the cell size during development, presumably by regulating recycling of the apical endosomes, MyosinVb-Rab 10 interaction regulates the apically directed transport from TGN downstream of the mTOR-FASN axis, during compensatory cell growth. Data are median ±interquartile range. **P*<0.05, ***P*<0.01, ****P*<0.001 (Kruskal–Wallis test with Dunn's post hoc test). ns, not significant. Note that only essential pairwise comparisons are shown in the figure panels B,D and F. For the complete list of pairwise comparisons please refer to Table S6. Scale bars: 20 µm (X-Y plane of A,C,E); 5 µm (Y-Z plane of C).

from the Golgi in Exon D morphants. However, in the absence of the Exon D isoform, the newly synthesized membrane lipids under the control of mTOR do not get transported to the apical domain but accumulate at the Golgi and presumably get rerouted to the basolateral domain, making the cells more columnar.

The mTOR activation and FASN upregulation is strongly linked with an increase in the trans-Golgi size as well as cell size. In addition, inhibition of mTOR, as well as FASN synthesis, results in a decrease in Golgi size and prevents cellular hypertrophy. Besides, though not revealed by the Rapamycin treatment, presumably due to weaker inhibition, Torin 1 treatment reveals that mTOR signaling is also essential for peridermal cell growth during development. These data suggest a linear relationship between mTOR-directed lipid synthesis and trans-Golgi morphology, and show that such trans-Golgi scaling is ancillary for cells to grow big, probably by allowing storage of additional membrane and facilitating regulated membrane transport towards increased requirement. Our data also reveal that Myosin Vb functions as a permissive step at the trans-Golgi surface, downstream to the membrane biogenesis step. Thus, the coordination between lipid synthesis and transport takes place at the trans-Golgi, which is a known sorting and trafficking hub of the cell.

Overall, our study reveals that interactions of Myosin Vb with Rab11 and Rab10 fine tune epithelial cell morphology during both development and compensatory cell growth.

MATERIALS AND METHODS

Ethics statement

Zebrafish rearing, handling and experimentation were carried out as per the guidelines recommended by the Committee for the Purpose of Control and Supervision of Experiments on Animals (CPCSEA), Government of India, and approved by the institutional animal ethics committee (TIFR/IAEC/2017-11).

Fish strains

We used *Tübingen* (*Tü*) strain and gsp^{NS042} allele of *goosepimples/myosin Vb* in this study (Sonal et al., 2014). Transgenic lines *Tg(cldnB:lynEGFP)* (Haas and Gilmour, 2006), $Tg\ (h2afx:EGFPRab11a)^{mw6}$ and $Tg(h2afx:EGFP\text{-}Rab7)^{mw7}$ (Clark et al., 2011) were used for experiments requiring visualization of plasma membrane, recycling endosomes and late endosomes, respectively.

Morpholino and plasmid injections

Myosin Vb splice site morpholino (250-300 pl of 200 µM) (Sonal et al., 2014), ΔNp63 morpholino (250-300 pl of 50 µM) (Bakkers et al., 2002), Myosin Vb Exon D splice site morpholino (5′-GCTTTACTGCCATCCGAGTGCAAGA-3′; 300-500 pl of 500 µM) (Liu et al., 2013) and its 5-base mismatch control (5′-GCTTTAGTCC-CATGCCAGTCCAAGA-3′) were microinjected in zebrafish embryos at the one-cell stage using PV830 Pneumatic PicoPump. We also used the second Exon D slice-site morpholino (5′-ACTGCCATCCGAGTGCAAGA-GAGCC-3′) for validation of the phenotype.

EGFP-GalT plasmid (500-600 pl of 50 ng/µl) was injected at the one-cell stage. This plasmid was generated by the Jennifer Lippincott-Schwartz lab (Addgene plasmid #11929) and previously used by the Lila Solnica-Krezel lab in zebrafish.

RNA synthesis and injections

For RNA rescue of *myosin Vb* morphants, both Exon D (+) and Exon D (−) isoforms of zebrafish *Myosin Vb* coding DNA sequences (CDS) were synthesized. Using Clustal Omega software (McWilliam et al., 2013), the zebrafish *myosin Vb* sequence was aligned with the human CDS (Roland et al., 2011) to determine the sites for introduction of mutations to abolish Rab11 binding (Fig. S1A). By introducing these mutations in both Exon D (+) and Exon D (−) isoforms, two additional $Rab11^{-/-}$ versions for D1705E and Q1739R in Exon D (+), and D1678E and Q1712R in Exon D (−) were synthesized (GeneArt, Thermo Fisher Scientific). All Myosin Vb constructs were synthesized in pMK vectors with additional restriction sites and a linker at 3′ terminal (GGAGGAAGCGGAGGAAGCGGAGGAGGAAGC) and sub-cloned into pCS2+8CmCherry and pCS2+8CeGFP vectors.

Following linearization of the plasmid, mRNA was synthesized using the SP6 mMessagemMachine *In-vitro* Transcription Kit (Thermo Fisher Scientific, AM1340) followed by mRNA purification using BioRad MicroBio-Spin columns P-30, Tris (732-6250) and eluted in nuclease-free water. For the rescue experiments, the desired RNA (1.2 nl of 65-75 ng/µl in nuclease-free distilled water) was injected in the cytoplasm at the one-cell stage before the Myosin Vb splice site morpholino injection. For clonal rescue in Exon D morphants, the Exon D morpholino was injected at the one-cell stage, followed by injecting 0.5-0.8 nl of mRNA for the desired Myosin Vb isoform (75 ng/µl) and Citrine mRNA (100 ng/µl) as a tracer in one of the cells at the 16-cell stage. The phenotypic rescues in embryos and clones were assessed at 40 hpf.

Rab10 CDS was synthesized (GeneArt, Thermo Fisher Scientific) and subcloned in pCS2+8NmCherry and pCS2+8NeGFP vectors with the same linker at the N-terminal of the gene as stated above. This plasmid was linearized and, post *in vitro* transcription, ∼1.2 nl of 120 ng/µl RNA was microinjected. pCS2+8NmCherry (Addgene plasmid #34936) and pCS2+8NeGFP (Addgene plasmid #34953) were gifts from Amro Hamdoun (Gökirmak et al., 2012).

RT-PCR for the validation of knockdown of the Exon D isoform

To confirm specific knockdown of the Exon D isoform, both control as well as Exon D morpholino-injected embryos (30-40 each) were fixed in TRIzol Reagent (Thermo Fisher Scientific, 15596026) at 48 hpf. Embryos were homogenized, stored at −80°C for 3-4 h and processed for RNA isolation. The RNA was dissolved in nuclease-free water and used to prepare cDNA using SuperScript™ IV First-Strand Synthesis System (Invitrogen, 18091050). PCR amplification of Myosin Vb along with Actin as a control from cDNA was performed using the following primers: Exon D FP 5′-CTCAACGTCAGAGGACGATATAAACG-3′, Exon D RP 5′-GTGAAGGGCTTCCAACTCATCC-3′ (sequence provided by Liu et al., 2013), Actin FP 5′-ATCACACCTTCTACAACGAGC-3′, Actin RP 5′-CATCACCAGAGTCCATCACG-3′.

Drug treatments

Embryos at 20 hpf were treated with 10 µM concentration of EGFR inhibitor PD168393 (Calbiochem, 513033) and 30 µg/ml Cerulenin (Sigma-Aldrich, C2389). Treatments with 2 µM Rapamycin (Santa Cruz Biotechnology, SC-3504), 5 µM Torin 1 (Abcam, ab218606) and 20 µM Compound C (Sigma-Aldrich, P5499) were started from 24 hpf. Rapamycin was changed once at 36 hpf. Before fixation at 48 hpf, embryos were given three washes of E3 (embryonic media) of 5 min each (without methylene blue). All the stocks were prepared in DMSO (Sigma-Aldrich, D8418). During treatments, DMSO

Development (2022) 149, dev199363. doi:10.1242/dev.199363

concentration was adjusted to 1% in the test and control samples. DMSO-treated wild-type embryos are used as controls in all drug experiments.

BODIPY C5-Ceramide, dextran and lysotracker assays

To mark the biogenic vesicles in the live periderm, embryos were pulsed with 3 µM BODIPY™ FL C5-Ceramide complexed to bovine serum albumin (Invitrogen, B22650) for 2.5 h at 29°C followed by three 5 min washes with E3, and chased in E3 for another 3 h before fixing at 36 hpf in 4% paraformaldehyde (PFA) in PEMTT (0.1 M PIPES, 5 mM EGTA, 2 mM $MgCl_2 \cdot 6H_2O$, 0.1% Triton X-100, 0.1% Tween 20, pH 6.8) (Song et al., 2013) overnight followed by serial glycerol upgradation (30%, 50% and 70%) preceding confocal imaging.

For endocytosis assays, the larvae were incubated in 50 µg/ml solution of 10 kDa Alexa 546-conjugated Dextran (Invitrogen, D-22911) in E3 for 3 h followed by washing and mounting for live imaging, or for 12 h followed by washing, PFA fixation and immunostaining for fixed imaging. For visualizing acidic compartments, embryos were incubated in 5 µM Lysotracker Red DND-99 (Invitrogen; L7528) in E3 for 3 h followed by washes with E3 and live imaging.

Immunostaining and WGA staining

Immunostainings were performed according to previously published protocol (Gupta and Sonawane, 2020). Briefly, embryos were fixed in 4% PFA in PBS followed by methanol post-fixation. For Rab7 immunostaining, fixation was carried out in 4% PFA in PEMTT. Embryos were permeabilized by washing in PBT, followed by blocking in 10% normal goat serum (NGS) in PBT and primary antibody treatment. The following primary antibodies were used in this study: rabbit anti-GFP (1:200, Torrey Pines Biolabs, TP401), 12A6 mouse anti-GFP (1:100, Developmental Studies Hybridoma Bank, 12A6), rabbit anti-RFP (1:200, Abcam, ab62341), rabbit anti-pS6 ribosomal protein (S240/244) (1:100, Cell Signaling Technology, 2214S), mouse anti-E cadherin (1:200, BD Biosciences, 610182), rabbit anti-FASN (1:100, Novus Biologicals, NB400-114), anti-acetylated tubulin (1:100, Sigma-Aldrich, T7451), rabbit anti-Rab10 (1:100, Sigma prestige, HPA045611). Primary antibodies were washed off, and embryos were incubated with secondary antibodies or fluorescent conjugates. The following secondary antibodies and fluorescent conjugates were used in this study: conjugated WGA Alexa Fluor 594 and 633 (1:200, Invitrogen, W11262 and W21404); Alexa 488 conjugated goat anti-rabbit IgG and goat anti-mouse IgG antibodies (1:250, Invitrogen, A-11034 and A-11029); Cy3- and Cy5-conjugated goat anti-rabbit IgG antibody (1:750, Jackson ImmunoResearch, 111-165-144 and 111-175-144); Cy3- and Cy5-conjugated goat anti-mouse IgG antibody (1:750, Jackson ImmunoResearch, 115-165-146 and 115-175-146) and Cy3-conjugated goat anti-rat IgG antibody (1:750, Jackson ImmunoResearch, 112-165-167). Post incubation, secondary antibodies were washed off and embryos were post fixed in 4% PFA followed by serial upgradation in glycerol.

Image acquisition

Brightfield images were taken on stereomicroscope (SteREO Discovery, Zeiss) mounted with AxioCam (Zeiss), after anesthetizing the embryos with 0.04% MESAB (Sigma-Aldrich, E10521) and mounting in low melting agarose (Sigma-Aldrich, A9414) on a glass slide.

For live imaging, embryos were anesthetized in 0.04% Tricaine solution in E3 buffer and mounted in a 35 mm glass bottom Petri dish in low melting agarose with the widest part of the dorsal head against the glass bottom. For fixed samples, embryo heads were dissected out and mounted on a glass slide in 70% glycerol, with the widest part of the dorsal head against the glass coverslip (Gupta and Sonawane, 2020). Imaging was performed on the dorsal head epidermis using Zeiss 710 and 880 confocal microscopes. For cell surface area quantifications, confocal stacks were obtained using EC neo-fluor 63×/1.3 oil objective with digital zoom 1.5, pinhole 1 AU, resolution 1024×1024, averaging 4, bit depth 16 and optimal slice interval of 0.378 µm. High sensitivity detectors on Zeiss 880 were used for visualizing Rab7-GFP and Rab10 mCherry localization. For imaging BODIPY™ FL C5-Ceramide, samples were subjected to λex=488 nm on Zeiss 710. The signal was collected simultaneously at λem ∼515 nm (green) and ∼620 nm (red) on two different tracks. Some of the images were optimized post acquisition for better representation by adjusting brightness/contrast equally for both control and test images.

Image analysis

Cell surface area quantification

To measure the total cell surface area of the peridermal cells, experiments were conducted using the *Tg(cldnB:lynEGFP)* line (Haas and Gilmour, 2006) and embryos were immunostained using anti-GFP and E-cadherin antibodies. To quantify surface area, cell outlines in each *z*-slice were manually traced, and area and perimeter were measured using the ImageJ measure function. The area of the top-first slice was estimated as the cross-section area and added to the ridge area to calculate the apical surface area. To quantify the ridge surface area, maximum intensity projection for the two apical slices spanning the approximate height of the microridges was smoothened and thresholded using an auto local thresholding function (Otsu method with radius 8 represented the microridges faithfully). Microridges for each cell were cropped out, converted to binary, and the perimeter was measured using the analyze particle function. The sum of the perimeter was then multiplied by two times the slice interval to obtain the total ridge area. To find out basolateral surface area, the perimeter of each slice starting with the first E-cadherin (basolateral marker) marked slice was measured by tracing GFP-marked membrane and multiplied by 0.378 (height of an optical *z*-slice in µm), and added to the surface area of the last slice. The apical and basolateral surface areas were summed to estimate the total cell surface area.

TGN volume and surface area quantification

We used *Tg(cldnB:lynEGFP)* line to mark the membrane for visualizing the cell boundaries of individual cells along with WGA as a TGN marker for these experiments. All images were deconvolved with Huygens Professional version 18.10 (Scientific Volume Imaging, http://svi.nl), and volume and surface area of the TGN were calculated using the following parameters: average background value=computed from the image, number of iterations=30, signal to noise ratio=20 and quality change threshold=0.01. These settings were kept constant across all the samples. GFP channel was used to crop the individual cells from the deconvoluted images and cropped cells were then surface rendered for WGA-marked TGN to quantify the volume and surface area of the TGN of each cell. The surface rendered images were compared with the original deconvolved images and visually checked for accurate representation. The deconvolved images of the TGN were then analyzed using the advanced object analyzer plugin (garbage volume=5 and threshold=10-12% were used for all experiments). The individual values of volume and surface area per object in the WGA channel were added to obtain total volume and surface area of the TGN, which were then plotted using GraphPad PRISM software.

Fluorescence intensity quantification

For estimation of the fluorescence intensity ratio for BODIPY C5-Ceramide staining, selected post-TGN vesicle boundaries were marked using the freehand selection tool and total intensity readings in each of the channels [λem ∼515 nm (green) and ∼620 nm (red)] were measured using the measure tool of the ImageJ software. The same selection mark was then placed on the adjoining TGN region chosen randomly from the same cell to calculate the intensity ratio. Equal number of vesicles and TGN regions were quantified per embryo.

For estimating mean fluorescent intensity for FASN, GFP-marked membrane was used to trace the cell boundaries in each *z*-slice of the confocal *z*-stack by using the freehand selection tool in the ImageJ software, and mean intensity measurements were recorded and summed for each cell.

Statistical analysis and graphs

Sigma Plot software was used for statistical analysis for all the quantitative tests. We used the Mann–Whitney test to compare the medians of two test groups, and the Kruskal–Wallis test with Dunn's post hoc test to compare medians of multiple test groups. The datasets represented by dot-plots

show medians with interquartile range, and those represented with bar graph show error bars denoting ±s.e.m. Graphs were plotted using GraphPad PRISM software. Detailed statistical comparisons are presented in Tables S1-S12).

The sample sizes were empirically determined based on our previous studies. The sample size (n) was sufficiently large to correctly and reproducibly parse out the difference and/or reveal the trend. No data were excluded during the statistical analysis. Only those experiments that failed owing to mRNA or morpholino quality, injection volumes or quality of embryos were not considered for further analysis. For the knockdown studies, rescue experiments, drug treatments and imaging, embryos were selected randomly. Absolutely no attempts were made to pre-select embryos based on any criterion. For quantification of cellular features, randomization was achieved by analyzing every alternate cell starting from the upper left corner. Most of the experiments were quantified with appropriate quantification methods eliminating any bias and requirement for the blind analysis. During statistical analysis, an *a priori* assessment of data parameters (e.g. normality and variance) was carried out to ensure that the data met the assumptions of the test used.

Details of number of experimental repeats, number of embryos imaged and number of cells analyzed for quantifications are listed in Table S13.

Acknowledgements
We thank Prof. Lila Solnica-Krezel and Prof. Brian Link for sharing reagents, Prof. Nagaraj Balasubramanian and Vibha Singh for suggestions on Golgi quantifications, Dr Kalidas Kohale for fish facility maintenance, Dr Mandar Phatak and Anusha Singh for their help in experiments.

Competing interests
The authors declare no competing or financial interests.

Author contributions
Conceptualization: K.G., M.S.; Methodology: K.G., S.M., S.S.; Formal analysis: K.G., S.M., S.S.; Investigation: K.G., S.M., S.S.; Writing - original draft: K.G.; Writing - review & editing: M.S., K.G.; Supervision: M.S.; Project administration: M.S.; Funding acquisition: M.S.

Funding
This study was funded by the Tata Institute of Fundamental Research [RTI4003 (12P-121)].

Peer review history
The peer review history is available online at https://journals.biologists.com/dev/article-lookup/doi/10.1242/dev.199363.

References
Al-Awqati, Q. (2015). Kidney growth and hypertrophy: the role of mTOR and vesicle trafficking. *J. Clin. Invest.* **125**, 2267-2270. doi:10.1172/JCI81508

Bakkers, J., Hild, M., Kramer, C., Furutani-Seiki, M. and Hammerschmidt, M. (2002). Zebrafish ΔNp63 is a direct target of Bmp signaling and encodes a transcriptional repressor blocking neural specification in the ventral ectoderm. *Dev. Cell* **2**, 617-627. doi:10.1016/S1534-5807(02)00163-6

Blom, T., Somerharju, P. and Ikonen, E. (2011). Synthesis and biosynthetic trafficking of membrane lipids. *Cold Spring Harb. Perspect. Biol.* **3**, a004713. doi:10.1101/cshperspect.a004713

Boehlke, C., Kotsis, F., Patel, V., Braeg, S., Voelker, H., Bredt, S., Beyer, T., Janusch, H., Hamann, C., Gödel, M. et al. (2010). Primary cilia regulate mTORC1 activity and cell size through Lkb1. *Nat. Cell Biol.* **12**, 1115-1122. doi:10.1038/ncb2117

Clark, B. S., Winter, M., Cohen, A. R. and Link, B. A. (2011). Generation of Rab-based transgenic lines for in vivo studies of endosome biology in zebrafish. *Dev. Dyn.* **240**, 2452-2465. doi:10.1002/dvdy.22758

D'Souza, Z., Blackburn, J. B., Kudlyk, T., Pokrovskaya, I. D. and Lupashin, V. V. (2019). Defects in COG-mediated Golgi trafficking alter endo-lysosomal system in human cells. *Front. Cell Dev. Biol.* **7**, 118. doi:10.3389/fcell.2019.00118

Eberlé, D., Hegarty, B., Bossard, P., Ferré, P. and Foufelle, F. (2004). SREBP transcription factors: master regulators of lipid homeostasis. *Biochimie* **86**, 839-848. doi:10.1016/j.biochi.2004.09.018

Engevik, A. C., Kaji, I., Postema, M. M., Faust, J. J., Meyer, A. R., Williams, J. A., Fitz, G. N., Tyska, M. J., Wilson, J. M. and Goldenring, J. R. (2019). Loss of myosin Vb promotes apical bulk endocytosis in neonatal enterocytes. *J. Cell Biol.* **218**, 3647-3662. doi:10.1083/jcb.201902063

Fediuc, S., Gaidhu, M. P. and Ceddia, R. B. (2006). Regulation of AMP-activated protein kinase and acetyl-CoA carboxylase phosphorylation by palmitate in skeletal muscle cells. *J. Lipid Res.* 47, 412-420. doi:10.1194/jlr.M500438-JLR200

Fernández-Galilea, M., Pérez-Matute, P., Prieto-Hontoria, P. L., Sáinz, N., López-Yoldi, M., Houssier, M., Martínez, J. A., Langin, D. and Moreno-Aliaga, M. J. (2014). α-Lipoic acid reduces fatty acid esterification and lipogenesis in adipocytes from overweight/obese subjects. *Obesity* **22**, 2210-2215. doi:10.1002/oby.20846

Ginzberg, M. B., Kafri, R. and Kirschner, M. (2015). On being the right (cell) size. *Science* **348**, 1245075. doi:10.1126/science.1245075

Gökirmak, T., Campanale, J. P., Shipp, L. E., Moy, G. W., Tao, H. and Hamdoun, A. (2012). Localization and substrate selectivity of sea urchin multidrug (MDR) efflux transporters. *J. Biol. Chem.* **287**, 43876-43883. doi:10.1074/jbc.M112.424879

Gómez-Gálvez, P., Vicente-Munuera, P., Tagua, A., Forja, C., Castro, A. M., Letrán, M., Valencia-Expósito, A., Grima, C., Bermúdez-Gallardo, M., Serrano-Pérez-Higueras, Ó. et al. (2018). Scutoids are a geometrical solution to three-dimensional packing of epithelia. *Nat. Commun.* **9**, 2960. doi:10.1038/s41467-018-05376-1

Griffiths, G. and Simons, K. (1986). The trans Golgi network: Sorting at the exit site of the Golgi complex. *Science* **234**, 438-443. doi:10.1126/science.2945253

Gupta, K. and Sonawane, M. (2020). CMV promoter-driven expression and visualization of tagged proteins in live and fixed zebrafish embryonic epidermis. *Exp. Protoc. Biotechnol.* **48**, 29-41. doi:10.1007/978-1-0716-0607-0_3

Haas, P. and Gilmour, D. (2006). Chemokine signaling mediates self-organizing tissue migration in the zebrafish lateral line. *Dev. Cell* **10**, 673-680. doi:10.1016/j.devcel.2006.02.019

Haga, S., Ogawa, W., Inoue, H., Terui, K., Ogino, T., Igarashi, R., Takeda, K., Akira, S., Enosawa, S., Furukawa, H. et al. (2005). Compensatory recovery of liver mass by Akt-mediated hepatocellular hypertrophy in liver-specific STAT3-deficient mice. *J. Hepatol.* **43**, 799-807. doi:10.1016/j.jhep.2005.03.027

Hannezo, E., Prost, J. and Joanny, J.-F. (2014). Theory of epithelial sheet morphology in three dimensions. *Proc. Natl. Acad. Sci. USA* **111**, 27-32. doi:10.1073/pnas.1312076111

Hobdy-Henderson, K. C., Hales, C. M., Lapierre, L. A., Cheney, R. E. and Goldenring, J. R. (2003). Dynamics of the apical plasma membrane recycling system during cell division. *Traffic* **4**, 681-693. doi:10.1034/j.1600-0854.2003.00124.x

Honda, H., Ogita, Y., Higuchi, S. and Kani, K. (1982). Cell movements in a living mammalian tissue: Long-term observation of individual cells in wounded corneal endothelia of cats. *J. Morphol.* **174**, 25-39. doi:10.1002/jmor.1051740104

Ikonen, E. and Simons, K. (1998). Protein and lipid sorting from the trans-Golgi network to the plasma membrane in polarized cells. *Semin. Cell Dev. Biol.* **9**, 503-509. doi:10.1006/scdb.1998.0258

Jones, K. T., Greer, E. R., Pearce, D. and Ashrafi, K. (2009). Rictor/torc2 regulates Caenorhabditis elegans fat storage, body size, and development through sgk-1. *PLoS Biol.* **7**, e1000060. doi:10.1371/journal.pbio.1000060

Kanazawa, T., Takematsu, H., Yamamoto, A., Yamamoto, H. and Kozutsumi, Y. (2008). Wheat germ agglutinin stains dispersed post-golgi vesicles after treatment with the cytokinesis inhibitor psychosine. *J. Cell. Physiol.* **215**, 517-525. doi:10.1002/jcp.21328

Kawaguchi, A., Tomoda, H., Nozoe, S., Omura, S. and Okuda, S. (1982). Mechanism of action of cerulenin on fatty acid synthetase: Effect of cerulenin on iodoacetamide-induced malonyl-coa decarboxylase activity. *J. Biochem.* **92**, 7-12. doi:10.1093/oxfordjournals.jbchem.a133933

Khandelwal, P., Prakasam, H. S., Clayton, D. R., Ruiz, W. G., Gallo, L. I., van Roekel, D., Lukianov, S., Peränen, J., Goldenring, J. R. and Apodaca, G. (2013). A Rab11a-Rab8a-Myo5B network promotes stretch-regulated exocytosis in bladder umbrella cells. *Mol. Biol. Cell* **24**, 1007-1019. doi:10.1091/mbc.e12-08-0568

Knobloch, M., Braun, S. M. G., Zurkirchen, L., von Schoultz, C., Zamboni, N., Araúzo-Bravo, M. J., Kovacs, W. J., Karalay, Ö., Suter, U., Machado, R. A. C. et al. (2013). Metabolic control of adult neural stem cell activity by Fasn-dependent lipogenesis. *Nature* **493**, 226-230. doi:10.1038/nature11689

Knowles, B. C., Roland, J. T., Krishnan, M., Tyska, M. J., Lapierre, L. A., Dickman, P. S., Goldenring, J. R. and Shub, M. D. (2014). Myosin Vb uncoupling from RAB8A and RAB11A elicits microvillus inclusion disease. *J. Clin. Invest.* **124**, 2947-2962. doi:10.1172/JCI71651

Kuo, Y., Huang, H., Cai, T. and Wang, T. (2015). Target of rapamycin complex 2 regulates cell growth via Myc in drosophila. *Sci. Rep.* **5**, 10339. doi:10.1038/srep10339

Lapierre, L. A., Kumar, R., Hales, C. M., Navarre, J., Bhartur, S. G., Burnette, J. O., Provance, D. W., Mercer, J. A., Bähler, M. and Goldenring, J. R. (2001). Myosin vb is associated with plasma membrane recycling systems. *Mol. Biol. Cell* **12**, 1843-1857. doi:10.1091/mbc.12.6.1843

Laplante, M. and Sabatini, D. M. (2009). mTOR signaling at a glance. *J. Cell Sci.* **122**, 3589-3594. doi:10.1242/jcs.051011

Lee, H. and Kimelman, D. (2002). A dominant-negative form of p63 is required for epidermal proliferation in zebrafish. *Dev. Cell* **2**, 607-616. doi:10.1016/S1534-5807(02)00166-1

Liu, Q., Chang, J. W., Wang, J., Kang, S. A., Thoreen, C. C., Markhard, A., Hur, W., Zhang, J., Sim, T., Sabatini, D. M. et al. (2010). Discovery of 1-(4-(4-propionylpiperazin-1-yl)-3-(trifluoromethyl)phenyl)-9-(quinolin-3-yl)benzo[h][1,6]-naphthyridin-2(1H)-one as a highly potent, selective mammalian target of rapamycin (mTOR) inhibitor for the treatment of cancer. *J. Med. Chem.* **53**, 7146-7155. doi:10.1021/jm101144f

Liu, Y., Xu, X.-H., Chen, Q., Wang, T., Deng, C.-Y., Song, B.-L., Du, J.-L. and Luo, Z.-G. (2013). Myosin Vb controls biogenesis of post-Golgi Rab10 carriers during axon development. *Nat. Commun.* **4**, 2005. doi:10.1038/ncomms3005

Lloyd, A. C. (2013). The regulation of cell size. *Cell* **154**, 1194-1205. doi:10.1016/j.cell.2013.08.053

Losick, V. P., Fox, D. T. and Spradling, A. C. (2013). Polyploidization and cell fusion contribute to wound healing in the adult Drosophila epithelium. *Curr. Biol.* **23**, 2224-2232. doi:10.1016/j.cub.2013.09.029

Madison, B. B. (2016). Srebp2: a master regulator of sterol and fatty acid synthesis. *J. Lipid Res.* **57**, 333-335. doi:10.1194/jlr.C066712

McWilliam, H., Li, W., Uludag, M., Squizzato, S., Park, Y. M., Buso, N., Cowley, A. P. and Lopez, R. (2013). Analysis tool web services from the EMBL-EBI. *Nucleic Acids Res.* **41**, W597-W600. doi:10.1093/nar/gkt376

Müller, T., Hess, M. W., Schiefermeier, N., Pfaller, K., Ebner, H. L., Heinz-Erian, P., Ponstingl, H., Partsch, J., Röllinghoff, B., Köhler, H. et al. (2008). MYO5B mutations cause microvillus inclusion disease and disrupt epithelial cell polarity. *Nat. Genet.* **40**, 1163-1165. doi:10.1038/ng.225

Nilsson, T., Pypaert, M., Hoe, M. H., Slusarewicz, P., Berger, E. G. and Warren, G. (1993). Overlapping distribution of two glycosyltransferases in the Golgi apparatus of HeLa cells. *J. Cell Biol.* **120**, 5-13. doi:10.1083/jcb.120.1.5

Omura, S. (1976). The antibiotic cerulenin, a novel tool for biochemistry as an inhibitor of fatty acid synthesis. *Bacteriol. Rev.* **40**, 681-697. doi:10.1128/br.40.3.681-697.1976

Pagano, R. E., Martin, O. C., Kang, H. C. and Haugland, R. P. (1991). A novel fluorescent ceramide analogue for studying membrane traffic in animal cells: accumulation at the Golgi apparatus results in altered spectral properties of the sphingolipid precursor. *J. Cell Biol.* **113**, 1267-1279. doi:10.1083/jcb.113.6.1267

Paoletti, L., Lu, Y.-J., Schujman, G. E., de Mendoza, D. and Rock, C. O. (2007). Coupling of fatty acid and phospholipid synthesis in Bacillus subtilis. *J. Bacteriol.* **189**, 5816-5824. doi:10.1128/JB.00602-07

Park, J.-A., Kim, J. H., Bi, D., Mitchel, J. A., Qazvini, N. T., Tantisira, K., Park, C. Y., McGill, M., Kim, S.-H., Gweon, B. et al. (2015). Unjamming and cell shape in the asthmatic airway epithelium. *Nat. Mater.* **14**, 1040-1048. doi:10.1038/nmat4357

Peterson, T. R., Sengupta, S. S., Harris, T. E., Carmack, A. E., Kang, S. A., Balderas, E., Guertin, D. A., Madden, K. L., Carpenter, A. E., Finck, B. N. et al. (2011). MTOR complex 1 regulates lipin 1 localization to control the srebp pathway. *Cell* **146**, 408-420. doi:10.1016/j.cell.2011.06.034

Phatak, M., Kulkarni, S., Miles, L. B., Anjum, N., Dworkin, S. and Sonawane, M. (2021). Grhl3 promotes retention of epidermal cells under endocytic stress to maintain epidermal architecture in zebrafish. *PLoS Genet.* **17**, e1009823. doi:10.1371/journal.pgen.1009823

Porstmann, T., Santos, C. R., Griffiths, B., Cully, M., Wu, M., Leevers, S., Griffiths, J. R., Chung, Y.-L. and Schulze, A. (2008). SREBP activity is regulated by mTORC1 and contributes to Akt-dependent cell growth. *Cell Metab.* **8**, 224-236. doi:10.1016/j.cmet.2008.07.007

Puliafito, A., Primo, L. and Celani, A. (2017). Cell-size distribution in epithelial tissue formation and homeostasis. *J. R. Soc. Interface* **14**, 20170032. doi:10.1098/rsif.2017.0032

Rabouille, C., Hui, N., Hunte, F., Kieckbusch, R., Berger, E. G., Warren, G. and Nilsson, T. (1995). Mapping the distribution of Golgi enzymes involved in the construction of complex oligosaccharides. *J. Cell Sci.* **108**, 1617-1627. doi:10.1242/jcs.108.4.1617

Razzell, W., Wood, W. and Martin, P. (2014). Recapitulation of morphogenetic cell shape changes enables wound re-epithelialisation. *Development* **141**, 1814-1820. doi:10.1242/dev.107045

Robenek, H. and Schmitz, G. (1991). Abnormal processing of Golgi elements and lysosomes in tangier disease. *Arterioscler. Thromb.* 11, 1007-1020. doi:10.1161/01.ATV.11.4.1007

Roland, J. T., Lapierre, L. A. and Goldenring, J. R. (2009). Alternative splicing in class v myosins determines association with rab10. *J. Biol. Chem.* **284**, 1213-1223. doi:10.1074/jbc.M805957200

Roland, J. T., Bryant, D. M., Datta, A., Itzen, A., Mostov, K. E. and Goldenring, J. R. (2011). Rab GTPase-Myo5B complexes control membrane recycling and epithelial polarization. *Proc. Natl. Acad. Sci. USA* **108**, 2789-2794. doi:10.1073/pnas.1010754108

Ruemmele, F. M., Mü, T., Schiefermeier, N., Ebner, H. L., Lechner, S., Pfaller, K., Thö, C. E., Goulet, O., Lacaille, F., Schmitz, J. et al. (2010). Loss-of-function of MYO5B is the main cause of microvillus inclusion disease: 15 novel mutations and a CaCo-2 RNAi cell model. *Hum. Mutat.* **31**, 544-551. doi:10.1002/humu.21224

Scaglia, N., Tyekucheva, S., Zadra, G., Photopoulos, C. and Loda, M. (2015). De novo fatty acid synthesis at the mitotic exit is required to complete cellular division. *Cell Cycle* **13**, 859-868. doi:10.4161/cc.27767

Schuller, H.-J., Hahn, A., Troster, F., Schutz, A. and Schweizer, E. (1992). Coordinate genetic control of yeast fatty acid synthase genes FAS1 and FAS2 by an upstream activation site common to genes involved in membrane lipid biosynthesis. *EMBO J.* **11**, 107-114. doi:10.1002/j.1460-2075.1992.tb05033.x

Sepich, D. S. and Solnica-Krezel, L. (2016). Intracellular Golgi Complex organization reveals tissue specific polarity during zebrafish embryogenesis. *Dev. Dyn.* **245**, 678-691. doi:10.1002/dvdy.24409

Sidhaye, J., Pinto, C. S., Dharap, S., Jacob, T., Bhargava, S. and Sonawane, M. (2016). The zebrafish goosepimples/myosin Vb mutant exhibits cellular attributes of human microvillus inclusion disease. *Mech. Dev.* **142**, 62-74. doi:10.1016/j.mod.2016.08.001

Soliman, G. A. (2011). The integral role of mTOR in lipid metabolism. *Cell Cycle* **10**, 861-862. doi:10.4161/cc.10.6.14930

Sonal, G. A., Sidhaye, J., Phatak, M., Banerjee, S., Mulay, A., Deshpande, O., Bhide, S., Jacob, T., Gehring, I., Nuesslein-Volhard, C. et al. (2014). Myosin Vb mediated plasma membrane homeostasis regulates peridermal cell size and maintains tissue homeostasis in the zebrafish epidermis. *PLoS Genet.* **10**, e1004614. doi:10.1371/journal.pgen.1004614

Song, S., Eckerle, S., Onichtchouk, D., Marrs, J. A., Nitschke, R. and Driever, W. (2013). Pou5f1-dependent EGF expression controls e-cadherin endocytosis, cell adhesion, and zebrafish epiboly movements. *Dev. Cell* **24**, 486-501. doi:10.1016/j.devcel.2013.01.016

Stefan, C. J., Trimble, W. S., Grinstein, S., Drin, G., Reinisch, K., De Camilli, P., Cohen, S., Valm, A. M., Lippincott-Schwartz, J., Levine, T. P. et al. (2017). Membrane dynamics and organelle biogenesis-lipid pipelines and vesicular carriers. *BMC Biol.* **15**, 102. doi:10.1186/s12915-017-0432-0

Sugimura, K. and Ishihara, S. (2013). The mechanical anisotropy in a tissue promotes ordering in hexagonal cell packing. *Development* **140**, 4091-4101. doi:10.1242/dev.094060

Swiatecka-Urban, A., Talebian, L., Kanno, E., Moreau-Marquis, S., Coutermarsh, B., Hansen, K., Karlson, K. H., Barnaby, R., Cheney, R. E., Langford, G. M. et al. (2007). Myosin Vb is required for trafficking of the cystic fibrosis transmembrane conductance regulator in Rab11a-specific apical recycling endosomes in polarized human airway epithelial cells. *J. Biol. Chem.* **282**, 23725-23736. doi:10.1074/jbc.M608531200

Tamori, Y. and Deng, W.-M. (2013). Tissue repair through cell competition and compensatory cellular hypertrophy in postmitotic epithelia. *Dev. Cell* **25**, 350-363. doi:10.1016/j.devcel.2013.04.013

Tamori, Y. and Deng, W.-M. (2014). Compensatory cellular hypertrophy: the other strategy for tissue homeostasis. *Trends Cell Biol.* **24**, 230-237. doi:10.1016/j.tcb.2013.10.005

Thoreen, C. C., Kang, S. A., Chang, J. W., Liu, Q., Zhang, J., Gao, Y., Reichling, L. J., Sim, T., Sabatini, D. M. and Gray, N. S. (2009). An ATP-competitive mammalian target of rapamycin inhibitor reveals rapamycin-resistant functions of mTORC1. *J. Biol. Chem.* **284**, 8023-8032. doi:10.1074/jbc.M900301200

Tumaneng, K., Russell, R. C. and Guan, K. L. (2012). Organ size control by Hippo and TOR pathways. *Curr. Biol.* **22**, R368-R379. doi:10.1016/j.cub.2012.03.003

Vadia, S., Tse, J. L., Lucena, R., Yang, Z., Kellogg, D. R., Wang, J. D. and Levin, P. A. (2017). Fatty acid availability sets cell envelope capacity and dictates microbial cell size. *Curr. Biol.* **27**, 1757-1767.e5. doi:10.1016/j.cub.2017.05.076

Vance, D., Goldberg, I., Mitsuhashi, O. and Bloch, K. (1972). Inhibition of fatty acid synthetases by the antibiotic cerulenin. *Biochem. Biophys. Res. Commun.* **48**, 649-656. doi:10.1016/0006-291X(72)90397-X

Vogel, G. F., Klee, K. M. C., Janecke, A. R., Müller, T., Hess, M. W. and Huber, L. A. (2015). Cargo-selective apical exocytosis in epithelial cells is conducted by Myo5B, Slp4a, Vamp7, and Syntaxin 3. *J. Cell Biol.* **211**, 587-604. doi:10.1083/jcb.201506112

Weis, V. G., Knowles, B. C., Choi, E., Goldstein, A. E., Williams, J. A., Manning, E. H., Roland, J. T., Lapierre, L. A. and Goldenring, J. R. (2016). Loss of MYO5B in mice recapitulates microvillus inclusion disease and reveals an apical trafficking pathway distinct to neonatal duodenum. *CMGH* **2**, 131-157. doi:10.1016/j.jcmgh.2015.11.009

Weisz, O. A. and Rodriguez-Boulan, E. (2009). Apical trafficking in epithelial cells: signals, clusters and motors. *J. Cell Sci.* **122**, 4253-4266. doi:10.1242/jcs.032615

Wen, X., Zeng, Y., Liu, L., Zhang, H., Xu, W., Li, N. and Jia, X. (2012). Zhenqing recipe alleviates diabetic nephropathy in experimental type 2 diabetic rats through suppression of SREBP-1c. *J. Ethnopharmacol.* **142**, 144-150. doi:10.1016/j.jep.2012.04.028

Yan, C., Wei, H., Minjuan, Z., Yan, X., Jingyue, Y., Wenchao, L. and Sheng, H. (2014). The mTOR inhibitor rapamycin synergizes with a fatty acid synthase inhibitor to induce cytotoxicity in ER/HER2-positive breast cancer cells. *PLoS ONE* **9**, e97697. doi:10.1371/journal.pone.0097697

Yao, Z., Davis, R. M., Kishony, R., Kahne, D. and Ruiz, N. (2012). Regulation of cell size in response to nutrient availability by fatty acid biosynthesis in Escherichia coli. *Proc. Natl. Acad. Sci. USA* **109**, E2561-E2568. doi:10.1073/pnas.1209742109

Yoon, S., Lee, M.-Y., Park, S. W., Moon, J.-S., Koh, Y.-K., Ahn, Y.-H., Park, B.-W. and Kim, K.-S. (2007). Up-regulation of acetyl-CoA carboxylase α and fatty acid synthase by human epidermal growth factor receptor 2 at the translational level in breast cancer cells. *J. Biol. Chem.* **282**, 26122-26131. doi:10.1074/jbc.M702854200

Zhang, C., Lu, J., Su, H., Yang, J. and Zhou, D. (2017). Fatty acid synthase cooperates with protrudin to facilitate membrane outgrowth of cellular protrusions. *Sci. Rep.* **7**, 46569. doi:10.1038/srep46569

Zhou, G., Myers, R., Li, Y., Chen, Y., Shen, X., Fenyk-Melody, J., Wu, M., Ventre, J., Doebber, T., Fujii, N. et al. (2001). Role of AMP-activated protein kinase in mechanism of metformin action. *J. Clin. Invest.* **108**, 1167-1174. doi:10.1172/JCI13505